Extended Reality for Deep Inferior Epigastric Perforator Breast Reconstruction

The BRAVER study

Killian Zijlstra

Delft University of Technology

TU Delft

Extended Reality for Deep Inferior Epigastric Perforator Breast Reconstruction

The BRAVER study

by

Killian Zijlstra

to obtain the degree of Master of Science
at the Delft University of Technology,
to be defended publicly on Monday July 8, 2024 at 09:30 AM.

Student number:	4652460	
Project duration:	November 20, 2023 – July 8, 2024	
Thesis committee:	Prof. dr. ir. H.H. Weinans,	TU Delft
	Dr. W. Maarse,	UMC Utrecht
	H.C. Nguyen, MSc.,	UMC Utrecht
	Dr. B.M.W. Cornelissen,	Erasmus MC

An electronic version of this thesis is available at http://repository.tudelft.nl/.

Cover image generated using DALL-E by OpenAI.

TU Delft

Preface

Before you lies my master thesis, the product of eight short months filled with learning and personal growth, for which I am deeply grateful. I have learned many things in the past seven years, but the most valuable lessons were learned outside of the lecture halls. I have very consciously enjoyed all the beautiful moments of my time as a student, and it feels like an enormous privilege to have experienced it all. Even though I am not yet sure what my future career will hold, I am eagerly looking forward to what lies ahead.

I owe thanks to many people who contributed to this project, but there are a few I would like to mention specifically. Firstly, I would like to express my gratitude to Chien for giving me the opportunity to embark on this research at the 3D Lab in the UMC Utrecht. Your guidance and belief in my capabilities have been a driving force behind my efforts. Wies, thank you for your time and supervision. Your availability, even amidst your busy schedule, and your insightful advice have been instrumental in shaping the direction and depth of my work. Harrie, I sincerely appreciate your constructive feedback and fresh perspective on my project. Your critical eye has significantly enhanced the quality of my research, pushing me to achieve higher standards. A special thanks goes to Eveline. Your introduction to reconstructive surgery and extended reality during my bachelor's studies sparked my interest and paved the way for this thesis. I would also like to extend my thanks to all the students of the 3D Lab. Your help, brainstorming sessions, and the fun times we shared made this journey not only productive but also enjoyable.

Lastly, my heartfelt appreciation and gratitude to my friends, family, and Lotte. Your unwavering support and encouragement have been my backbone, enabling me to persevere and achieve my goals. Without you, my accomplishments would not have been possible, let alone meaningful.

With sincere gratitude,

Killian Zijlstra
Rotterdam, June 2024

Summary

Background: Extended Reality (XR) has demonstrated significant improvements in multiple surgical specialties by reducing operative times and enhancing surgical outcomes. Nevertheless, its usability for perforator visualization in deep inferior epigastric perforator (DIEP) breast reconstruction remains largely unexplored.

Objective: The primary aim of this study was to assess the usability and potential added value of XR in DIEP flap breast reconstruction to enhance the three-dimensional understanding of the deep inferior epigastric artery and its perforators. The secondary objective of this study was to determine if the weight of DIEP flaps can be accurately estimated through the virtual model required for XR visualization.

Methods: This multicenter pilot study involved plastic surgeons and patients undergoing DIEP flap breast reconstruction at three Dutch medical centers. Abdominal computed tomography angiography (CTA) images were used to create virtual 3D models. Surgeons utilized the HoloLens 2 (Microsoft Corporation) to compare intraoperative findings regarding perforator caliber, location within the flap, and the intramuscular course of perforators against CTA. Usability was assessed via the System Usability Scale (SUS). The SUS, perforator characteristics, and the added value of XR in addition to CTA for preoperative planning of DIEP flap breast reconstruction were scored using a 5-point Likert scale with a minimum score of 1 and a maximum score of 5. Furthermore, DIEP flap weight estimations were derived from the segmentations of the DIEP flap required for the virtual model and compared with a two-dimensional method for DIEP flap weight predictions extracted from literature.

Results: This study presents the preliminary results. Up until now, five patients and surgeons have been included. SUS scores were 66 for CTA and 70 for XR, meaning both visualization methods have 'Good' usability. XR scored slightly higher compared to CTA regarding perforator caliber with median scores of 3 for CTA and 4 for XR. Location within the flap yielded median scores of 4 for CTA and 5 for XR. The median score for the intramuscular course was 4 for both CTA and XR. The median scores for utilizing XR in addition to CTA for preoperative planning of DIEP flap breast reconstruction and recommending it to a colleague were both 4. DIEP flap weight prediction derived from the virtual model compared to true flap weight showed a mean difference of 333 grams and a mean percentage difference of 18.9%, whereas the two-dimensional method showed a mean difference of 937 grams and a mean percentage difference of 44.5%.

Conclusion: The preliminary results from this study indicate that XR technology, using the HoloLens 2, is a feasible and potentially advantageous tool for preoperative planning in DIEP flap breast reconstruction. The usability of XR was found to be comparable to CTA, with slightly better performance in visualizing perforator characteristics. The positive feedback from participating surgeons suggests that XR could enhance the understanding of the DIEA and its perforators, potentially improving surgical outcomes. Accurate prediction of DIEP flap weight based on the virtual model using the methodology employed in this study is currently not feasible.

Keywords

Autologous Breast Reconstruction, Reconstructive Surgery, Plastic Surgery, 3D Medical Technology, Augmented Reality, Usability testing

Contents

Nomenclature

Abbreviations

Abbreviation	Definition
2D	Two-dimensional
3D	Three-dimensional
ABR	Autologous breast reconstruction
AR	Augmented reality
BMI	Body mass index
BR	Breast reconstruction
BRAVER	Breast Reconstruction And Visualization with Extended Reality
CTA	Computed tomography angiography
DIEA	Deep inferior epigastric artery
DIEP	Deep inferior epigastric perforator
EPD	Electronic patient record
HR-QoL	Health-related quality of life
IBR	Implant-based breast reconstruction
LAP	Lumbar artery perforator
LD	Latissimus dorsi
MR	Mixed reality
MR-A	Magnetic resonance angiography
MRI	Magnetic resonance imaging
PACS	Picture archiving and communication system
PAP	Profunda artery perforator
SD	Standard deviation
SUS	System usability scale
TRAM	Transverse rectus abdominis myocutaneous
USE	Usefulness, satisfaction, and ease of use
VR	Virtual reality
XR	Extended reality

1

Introduction

Breast cancer is the most frequently diagnosed cancer among women in the world [1]. Treatment often requires a multimodal approach, which may include (neo)adjuvant systemic therapy, surgery, and radiotherapy. Post-mastectomy breast reconstruction has become an essential part of treatment, as it significantly improves health-related quality of life (HR-QoL), body image, and sexual well-being. These benefits are especially pronounced when the reconstruction is done in the same surgery as the mastectomy, known as immediate reconstruction [2–4].

Breast reconstruction (BR) is categorized into implant-based breast reconstruction (IBR) and autologous breast reconstruction (ABR), including free flaps, pedicled flaps, and lipofilling. While IBR is generally quicker, less complex, and has no donor site morbidity, ABR tends to yield higher patient satisfaction in terms of satisfaction with the outcome of the breast, psychological well-being, and sexual well-being [5].

Numerous donor site regions have been described for ABR [6–11]. Examples of these are the latissimus dorsi (LD) flap, profunda artery perforator (PAP) flap, and the lumbar artery perforator (LAP) flap. Abdominal-based free tissue flaps, such as the deep inferior epigastric perforator (DIEP) and the transverse rectus abdominis myocutaneous (TRAM) flap, are regarded as favorable over other donor site regions due to the natural appearance, tissue quality of the abdomen, and donor site surplus [12, 13]. Figure 1.1 provides an illustrative overview of multiple reconstructive options and donor sites.

To be eligible for abdominal free flap ABR, patients need to have sufficient abdominal adipose tissue. Current methods depend on the surgeon's experience and a subjective pinch test examination with significant variation between different observers. Clinical assessments often underestimate the available volume of abdominal tissue, potentially discouraging less experienced surgeons from considering the abdominal donor site [14]. Multiple methods have been described that use CTA or MR-A images to predict flap weight [15–18]. However, none of these prediction methods have been widely implemented in clinical practice, potentially due to additional imaging and workload.

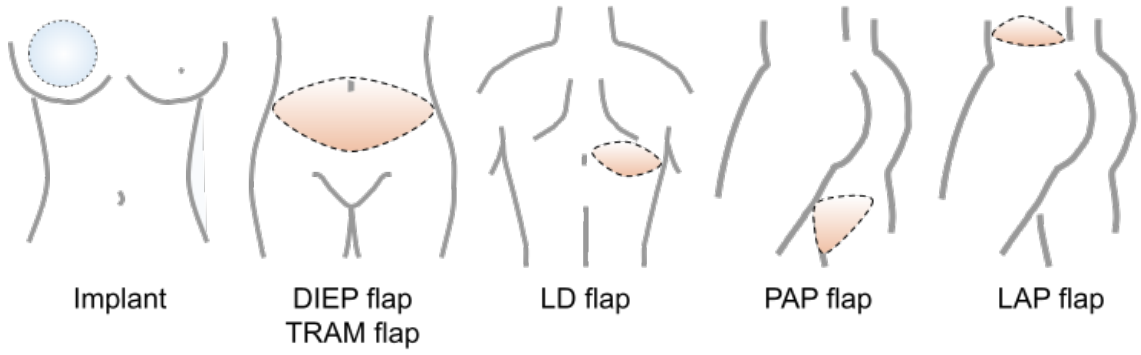

Figure 1.1: Implant-based breast reconstruction and multiple donor sites for autologous reconstruction.

Allen and Treece first described DIEP flap BR in 1994 [19]. Unlike the TRAM flap that uses muscle tissue along with skin and fat, the DIEP flap preserves the rectus abdominis muscle, reducing the risk of abdominal wall weakness or hernias. The DIEP flap is considered the gold standard and is by far the most used procedure for ABR worldwide. The procedure involves microsurgery to reconnect the blood vessels from the DIEP flap to the chest, ensuring a reliable blood supply for the transplanted tissue. The skin and fat tissue from the abdomen are shaped to create a natural-looking breast at the recipient site. Figure 1.2 contains a schematic overview of unilateral delayed DIEP flap BR.

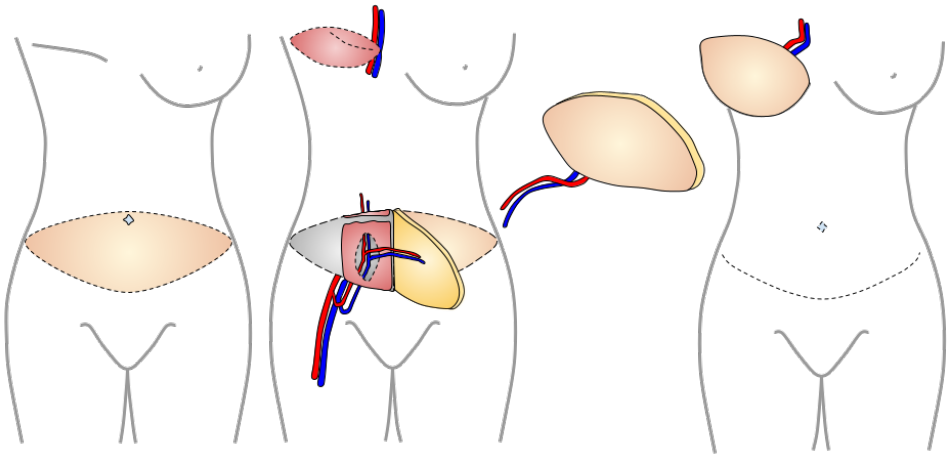

Figure 1.2: Schematic illustration of unilateral delayed DIEP breast reconstruction. Left:The abdominal donor site is highlighted. Middle: The rectus abdominis muscle is split, and a hemi-flap with a single perforator is lifted. At the chest, the pectoralis major is split to access the vessels at the recipient site. Right: The DIEP flap is connected to the internal mammary artery and vein. The abdomen is then closed, and the umbilicus is reconstructed.

Despite being the gold standard, DIEP flap BR is one of the most technically challenging and time-consuming procedures for BR. These difficulties increase the risk of perioperative complications. Consequently, surgeons are continually working to refine this surgical technique to reduce complication rates and operative times.

One of the most time-consuming aspects of DIEP flap BR is the flap dissection and selection of the most suitable perforators. These perforators stem from the deep inferior epigastric artery (DIEA), which then penetrate the rectus abdominis muscle into the subcutaneous fat of the abdomen. The branching pattern of this DIEA is known to have high variability, as first described by Moon and Taylor in 1988 [20]. Later adjustments by Rozen et al. provided a more complete description of the different types and prevalence of branching patterns [21]. Figure 1.3 has a schematic overview of the different branching patterns of the deep inferior epigastric artery and its prevalence according to Rozen et al. [21].

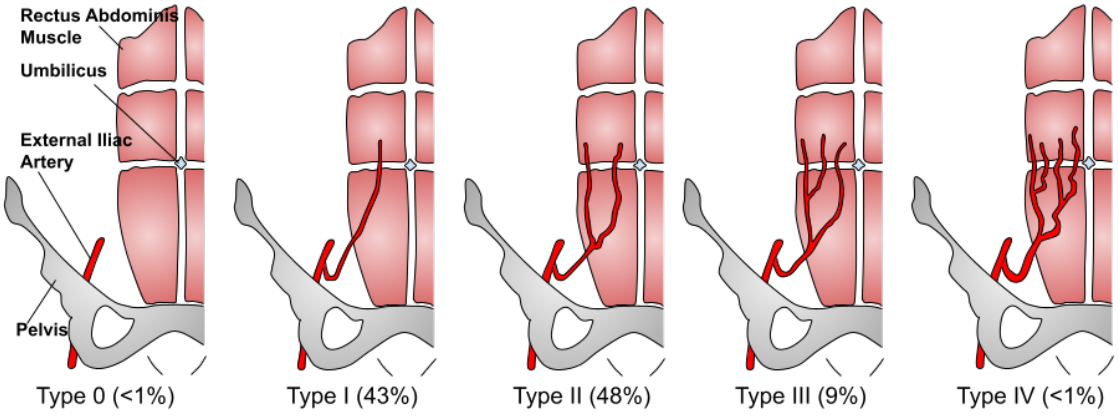

Figure 1.3: Schematic drawing of posterior view of branching patterns of the deep inferior epigastric artery. Adapted from Moon and Taylor 1998 and Rozen et al. 2010 [20, 21]

The variability in the branching pattern of the DIEA contributes to the challenge of identifying the most suitable perforator(s) for DIEP flap BR. The operative success of DIEP flap BR is related to the perioperative identification of the most suitable and dominant perforator(s) in terms of laterality, caliber, and intramuscular course. Ideal perforators typically have a relatively large caliber, a medial location within the flap, and a short intramuscular course [22]. Additionally, the most suitable perforator(s) should minimize muscle and nerve damage to prevent complications such as abdominal bulging, which has a prevalence of approximately 6.6% after DIEP flap BR. It has been observed that, when possible, using medial row perforators rather than lateral row perforators results in less abdominal bulging [23].

Computed tomography angiography (CTA) is the gold standard for preoperative imaging of the most suitable perforators [24–26]. Additionally, magnetic resonance imaging or angiography (MRI, MR-A) can be used for perforator identification [27, 28]. CTA and MR-A continue to display two-dimensional (2D) images in different planar views on a flat screen and provide no three-dimensional (3D) visualization of the perforators and other relevant structures. Stereoscopic 3D visualization is likely to enhance the ability of the surgeon to evaluate key aspects of the most suitable perforator, including its course and location within the flap [29].

To further enhance 3D understanding in perioperative planning of autologous free flap BR, the introduction of extended reality (XR) presents a promising improvement. XR is an umbrella term that includes augmented reality (AR), virtual reality (VR), and mixed reality (MR). These technologies allow users to immerse themselves and interact with 3D computer-simulated environments, ranging from full immersion in a virtual setting to subtle augmentations within the physical world [30]. Figure 1.4 illustrates the spectrum of extended reality.

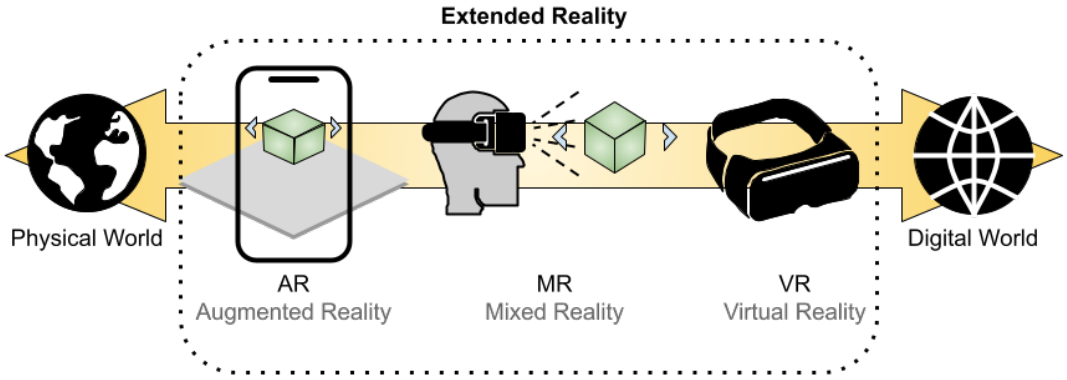

Figure 1.4: The spectrum of Extended Reality (XR): From small adjustments or projections of the physical world (AR) to interaction (MR) to complete immersion in the digital world (VR).

XR facilitates the stereoscopic 3D visualization of conventional 2D images that can aid the surgeon in the field of reconstructive surgery [31, 32]. The perioperative use of XR in other surgical specialties enhanced the 3D understanding of key anatomical sites, which led to an improved understanding of complex vasculature, allowing for safe vessel control during surgery and a reduction of operative time [33, 34].

Currently, multiple studies have assessed different aspects of XR for perioperative perforator visualization of DIEP flap BR and show promising results in terms of accurate perforator identification and operative time reduction [29, 35–42]. Figure 1.5 provides a schematic overview of the different modalities of XR described in the literature for DIEP flap BR.

To date, Berger et al. are one of the few researchers who have aimed to evaluate the usability of XR in DIEP flap BR [41]. However, this study did not create a virtual 3D model of the preoperative images like the other studies assessing XR for ABR. Instead, the study projected the 2D MR-A images onto the patient. Furthermore, this study only used two surgeons and one resident to assess the usability, where the minimum number of participants for usability studies is generally regarded as five [43–45]. For these reasons, the findings of this usability study do not accurately reflect the overall usability of XR in DIEP flap BR.

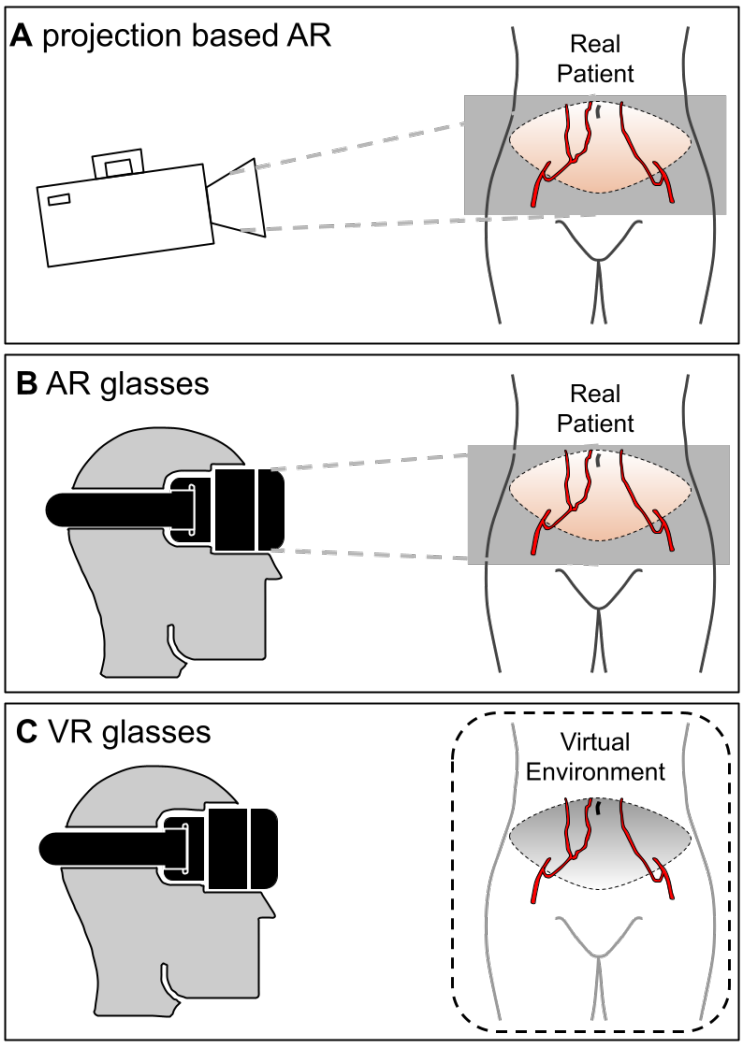

Figure 1.5: Extended Reality modalities used for DIEP flap breast reconstruction. A: Projection-based augmented reality glasses. B: Augmented reality glasses. C: Virtual reality glasses. The right DIEA has type II anatomy, the left DIEA has type I anatomy.

Objectives

The aim of this master thesis was twofold. The primary aim of this study was to assess the usability and potential added value of XR in DIEP flap breast reconstruction to enhance the 3D understanding of the DIEA and its perforators, as experienced by surgeons.

The secondary objective of this study was to determine if the weight of DIEP flaps can be accurately estimated through the virtual 3D model required for XR visualization.

2

Methods

2.1. Usability

2.1.1. Study design

This multicenter pilot study was conducted at the University Medical Center Utrecht (UMCU), the Erasmus Medical Center (EMC) Rotterdam, and the Amsterdam University Medical Center (Amsterdam UMC), all three located in the Netherlands. The study was approved by the internal board of the UMC Utrecht under number 23U-0720. Data collection started on April 1^{st}, 2023, and is currently still taking place. The goal is to include ten staff members and senior residents of the Department of Plastic, Reconstructive, and Hand Surgery and ten patients undergoing DIEP flap BR in this study.

2.1.2. Questionnaire

To evaluate the usability of CTA and XR, the System Usability Scale (SUS) developed by Brooke et al. was employed [46]. The SUS comprises 10 items and employs a 5-point Likert scoring system. Each item is scored on a scale ranging from 1 to 5, with 1 indicating ”Strongly Disagree” and 5 indicating ”Strongly Agree.” Figure 2.1 illustrates such a 5-point Likert scoring system.

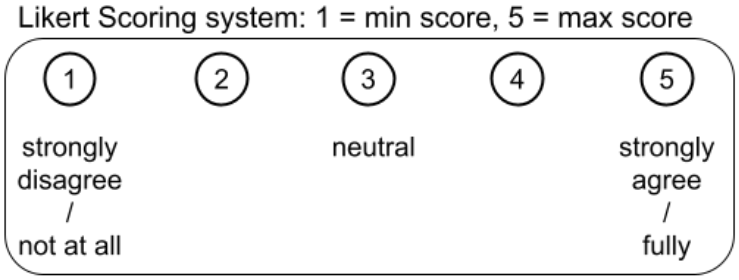

Figure 2.1: 5-point Likert Scoring scale used in this study.

The items of the SUS are phrased alternately in positive and negative terms to prevent response bias. This method requires respondents to carefully read each statement and thoughtfully consider whether they agree or disagree. The alternate phrasing necessitates a different scoring system for negative and positive items. For items 1, 3, 5, 7, and 9, the score contribution is the scale position minus one. For items 2, 4, 6, 8, and 10, the contribution is five minus the scale position. Next, the sum of the scores is multiplied by 2.5 to obtain the overall value of the SUS. SUS scores range from 0 to 100, with a higher score indicating better usability [46].

The SUS is technology agnostic, meaning it can be used for any type of system or software. To determine what aspects of XR possess potential added value, more specific questions regarding perforator characteristics were assessed. A questionnaire was created in collaboration with a staff member (WM)

from the Department of Plastic, Reconstructive, and Hand Surgery at UMC Utrecht, which consisted of three main parts: the SUS, perforator characteristics, and the added value of XR in addition to CTA.

The following questions regarding perforator characteristics required the surgeon to compare perforator caliber, location within the flap, and intramuscular course to intraoperative findings for both CTA and XR. The questions were scored using a similar 5-point Likert scoring system as the SUS and were identical for CTA and XR for comparability. A minimum score of 1 indicated that the visualization method (CTA or XR) was not at all comparable to intraoperative findings, while a maximum score of 5 indicated that the intraoperative findings were fully comparable to the visualization method.

1. (CTA / XR) provided a good understanding of the following perforator characteristics compared to intraoperative findings:
   (a) Location in the flap
   (b) Caliber
   (c) Intramuscular course

The questionnaire concluded with two final questions regarding the added value of XR in addition to CTA:

1. I would like to use an XR model in addition to CTA as it would improve planning of DIEP breast reconstruction.
2. I would recommend the use of XR for preoperative visualisation in addition to CTA for DIEP breast reconstruction to my peers.

These items were again assessed using the same 5-point Likert scale, where 1 represented 'not at all' and 5 represented 'fully.' Scores of 1 and 2 were interpreted as a negative opinion about XR, 3 as neutral, and 4 and 5 as positive. The complete questionnaire can be found in Appendix A.

2.1.3. Study procedures

Image acquisition

Patients scheduled for DIEP flap BR underwent abdominal CTA according to standard practice at their respective sites. The CTA images from the UMC Utrecht were made using different Philips CT scanners (Philips CT 7500 or Philips IQon spectral CT) using a tube voltage of $120\,\mathrm{kV}$ and a reference tube current of 20 - $500\,\mathrm{mAs}$. The images have a slice thickness of $0.9\,\mathrm{mm}$. $90\,\mathrm{mL}$ of Omnipaque $300\,\mathrm{mg}$ Iodine / mL was used as a contrast agent.

Creation of virtual 3D model

At the preoperative consultation in the outpatient clinic, patients were asked for informed consent to participate in this study. After informed consent was obtained, the abdominal CTA was extracted from the Picture Archiving and Communication System (PACS). The CTA images were pseudonymized and stored in DICOM format. From these CTA images, segmentations of the rectus abdominis muscle, pelvis, skin, DIEP flap, DIEA, and its perforators were created using Mimics 26.0 (Materialise NV, Belgium). The full segmentation protocol can be found in Appendix B.

The segmentations created from the CTA make up the virtual 3D model of the abdominal donor site and were created prior to surgery. This approach ensured that the virtual 3D model was verified by a second independent observer to check for any segmentation inaccuracies in a timely manner, allowing the surgeon to review the virtual 3D model directly after surgery.

CTA visualization

The surgery took place according to standard practice at the respective site. Immediately following surgery, the surgeon who performed the dissection of the DIEP flap participated in the following post-operative assessment:

The abdominal CTA was presented in PACS on a standard monitor, similar to the standard preoperative assessment of the CTA for DIEP flap BR. The surgeon was prompted to evaluate the intraoperatively identified perforators compared to the CTA in terms of caliber, location within the flap, and intramuscular course.

Subsequently, the questions regarding the usability and perforator characteristics of CTA were conducted. The collection and organization of the questionnaire responses were managed with the electronic data capture system Castor EDC.

XR visualization

Directly after completing the CTA assessment, the protocol moved to XR visualization. The HoloLens 2 (Microsoft Corporation) served as the XR modality. The virtual 3D model was visualized within the HoloLens using the Mimics Viewer (Materialise NV, Belgium) application.

A brief introduction to the HoloLens 2 and Mimics Viewer controls was provided, which took approximately one minute. Participants were then allowed to freely inspect and interact with the model according to their preferences. There were no time constraints imposed for the inspection of the XR model.

The opacity of all objects in the Mimics Viewer could be adjusted from fully opaque to fully transparent. Participants were asked to evaluate the perforators as they would on a conventional CTA when preparing for surgery. They were asked to focus on perforator caliber, intramuscular course, and location within the flap.

Lastly, the questionnaire proceeded with the usability, perforator characteristics, and opinion on the incorporation of XR in preoperative planning for DIEP flap BR. A flowchart depicting the methodology of this study is presented in Figure 2.2.

2.1.4. Study population

Patients included in this study were women above the age of 18 years scheduled for uni- or bilateral and immediate or delayed DIEP flap BR. To be eligible for this study, patients were required to have sufficient knowledge of the Dutch language to sign informed consent, and abdominal CTA imaging must indicate eligible perforators for DIEP flap BR. Exclusion criteria in this study were patients not eligible for DIEP flap BR, limited in their communication, or unable to provide informed consent.

2.1.5. Data extraction

The following participant characteristics were extracted from the electronic patient record (EPD) and the surgery report: age, body mass index (BMI), smoking status, uni- or bilateral reconstruction, immediate or delayed reconstruction, total operative time, flap ischemia time, (if applicable) mastectomy tissue weight, total abdominal flap weight (the combined weight of the left and right DIEP flaps before augmentation to match the contour of the breast mound), and the breast mound flap weight (the weight of a single DIEP flap after augmentation to match the contour of the breast mound). These descriptive results provide a comprehensive overview of the study population and the surgical procedures performed.

Additionally, the time required to create the virtual 3D model from the CTA images was recorded, as model creation time is crucial to evaluate before XR can be widely implemented in clinical practice for DIEP flap BR.

2.1.6. Data interpretation

The resulting SUS scores from the CTA and XR will be interpreted according to the adjective rating scale as described by Bangor et al. [47]. This will provide an indication of the usability of CTA and XR as experienced by the surgeon. Given the exploratory nature of this pilot study, which aimed to gather surgeons' opinions, no statistical analysis was performed to determine differences in usability or perforator characteristics.

The intraoperative findings regarding perforator characteristics were compared with those from CTA and the XR model, and the median, mode, and range were calculated and visualized.

The final two questions asked whether surgeons would want to use XR in addition to CTA and if they would recommend XR to a colleague. The median, mode, and range of the responses were calculated and visualized, with scores of 1 and 2 interpreted as a negative opinion about XR, 3 as neutral, and 4 and 5 as a positive opinion about XR.

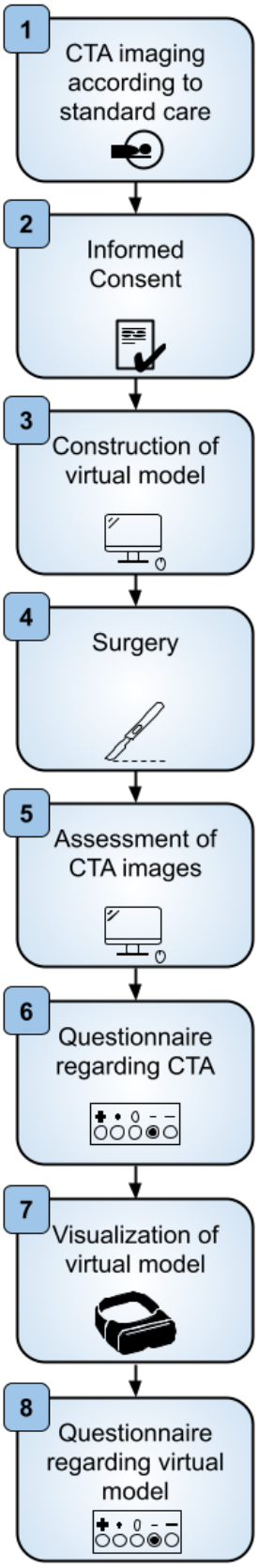

Figure 2.2: Flowchart of the methodology.

2.2. DIEP flap weight

2.2.1. Virtual 3D model

For the assessment of the secondary outcome measure, the DIEP flap weight was derived from the segmentation of the DIEP flap required for the virtual 3D model. The segmentation software Mimics 26.0 (Materialise NV, Belgium) automatically determines the volume of segmentations using the voxel size of the medical images and the number of voxels within the segmentation.

The reference points for determining the borders of the DIEP flap were established in collaboration with a surgeon (DK) from the Department of Plastic, Reconstructive, and Hand Surgery at UMC Utrecht.

The superior point of the DIEP flap was set at 1 cm above the center of the umbilicus. The inferior point was set at 7 cm above the introitus, preferably within the natural fold of the adipose tissue and skin. To determine the lateral borders of the DIEP flap, a dorsolateral line of 7 cm was drawn from the anterior superior iliac spine on the skin. From the end of this line, a new line was constructed 3 cm cranially. This procedure was repeated for the contralateral side, establishing the left and right lateral borders of the DIEP flap. The full segmentation protocol can be found in Appendix A.

2.2.2. 2D method

Additionally, the method described by Nanidis et al. for predicting DIEP flap weight, hereafter referred to as the 2D method, was used to compare the weight estimation of the virtual 3D model [14]. This 2D method was chosen because the authors describe it as having only an average percentage error of 6.38% and not differing significantly from the true flap weight. Moreover, it is the only method identified in the literature that is easily reproducible and does not require any additional imaging.

The 2D method from Nanidis et al. used three measurements obtained from the axial and sagittal CTA images [14]. Both sides of the abdominal donor site were considered as an isosceles prism as illustrated in Figure 2.3.

In the sagittal view, the base (b) of the flap was measured from the inferior edge of the umbilicus to the superior aspect of the symphysis pubis. In the axial view, the images were scrolled down until the sacral promontory flattened. This axial slice was used for both subsequent measurements. To measure the height (h) of the flap, a line was drawn at 45° from the lateral edge of the anterior superior iliac spine until the skin was reached (point A). The height (h) of the flap was then measured from point A to the abdominal skin in the midline. On the same image, the thickness (t) of the flap was measured in the midline from the skin to the linea alba. These measurements are depicted in Figure 2.4.

The combined flap volume of the left and right sides of the abdominal donor site is then calculated using formula 2.1.

$$\text{Flap volume} = b \times h \times t \tag{2.1}$$

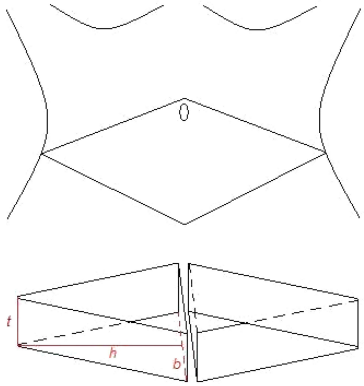

Figure 2.3: Schematic representation of the geometry of the abdominal flap and its resemblance to a double opposing triangular prism. Base (b), height (h), and thickness (t).
Extracted from: Nanidis TG, Ridha H, Jallali N. The use of computed tomography for the estimation of DIEP flap weights in breast reconstruction: a simple mathematical formula. J Plast Reconstr Aesthet Surg. 2014;67(10):1352–6. [14]

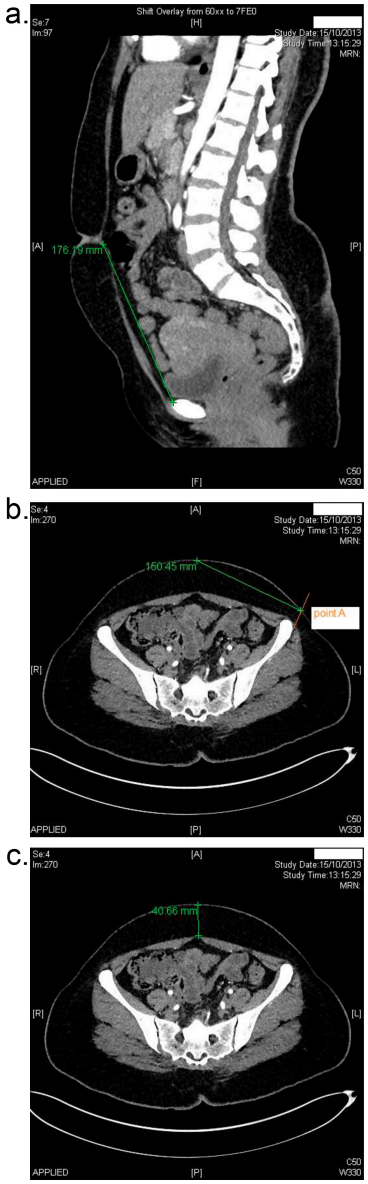

Figure 2.4: Depiction of how the parameters of the prism are measured using a patient's CT angiogram. a. Measurement of the base using the midline sagittal view. b. Measurement of the height using an axial slice at the level of the anterior superior iliac spines and the sacral promontory. c. Thickness of the flap measured on the same axial slice as b from the skin to the linea alba.
Extracted from: Nanidis TG, Ridha H, Jallali N. The use of computed tomography for the estimation of DIEP flap weights in breast reconstruction: a simple mathematical formula. J Plast Reconstr Aesthet Surg. 2014;67(10):1352–6. [14]

2.2.3. Data interpretation

The density of tissue within the DIEP flap used in literature is $1.0\,\mathrm{g\,cm^{-3}}$ meaning DIEP flap volume (in $\mathrm{cm^3}$) is numerically equal to its weight (in g) [14–18, 36]. To assess whether the estimation of DIEP flap weight of the virtual 3D model is accurate, the difference and percentage difference between the true DIEP flap weight and estimated DIEP flap weight is calculated and compared with the 2D method described by Nanidis et al. [14]. Percentage difference was calculated using formula 2.2.

$$\text{Percentage difference} = \frac{|\text{True Weight} - \text{Estimated Weight}|}{\text{True Weight}} \times 100\% \tag{2.2}$$

3

Results

3.1. Usability

The results presented in this master thesis regarding the usability of XR for perforator visualization in DIEP flap BR are the preliminary results of the larger Breast Reconstruction And Visualization with Extended Reality (BRAVER) study.

3.1.1. Participant characteristics

To date, five patients have been included in this study. The mean age of the participants was 55 years (range: 37–68) and the mean BMI was 28.4 $\mathrm{kg/m^2}$ (range: 23.7–30.6). None of the patients were smokers. Of the five patients, two underwent delayed unilateral BR, one received delayed bilateral BR, and two underwent immediate bilateral BR, resulting in a total of eight flaps used for reconstruction.

The mean operative time was 337 minutes (range: 263–411) for unilateral reconstruction and 504 minutes (range: 428–603) for bilateral reconstruction. The mean flap ischemia time was 56 minutes (range: 36–81). The mean total abdominal flap weight (the weight of the right and left side of the DIEP flap combined) was 1712 grams (range: 1030–2500). The mean weight of the breast mound flap used for the final reconstruction was 844 grams (range: 555–1075).

Surgeons included in this study were three staff members and two senior residents from the Department of Plastic, Reconstructive, and Hand Surgery at UMC Utrecht. The detailed participant characteristics are summarized in Table 3.1.

3.1.2. XR visualization

The construction of the virtual 3D model took approximately 5 hours for each participant, of which the greatest portion was devoted to the semi-automatic segmentation of the DIEA and the perforators. Figure 3.1 illustrates the final virtual 3D model as seen in the Mimics Viewer environment on a standard monitor. Figures 3.2 and 3.3 depict the virtual model as seen by the observer through the HoloLens 2.

Table 3.1: Participant characteristics

Participant	1	2	3	4	5	**Mean**
Age (y)	59	63	68	37	48	**55**
BMI (kg/m^2)	29.4	29.06	23.7	30.6	29.4	**28.4**
Smoking status	Non-smoking	Non-smoking	Non-smoking	Non-smoking	Non-smoking	
Uni- or bilateral	Unilateral	Bilateral	Unilateral	Bilateral	Bilateral	
Immediate or delayed	Delayed	Delayed	Delayed	Immediate	Immediate	
Total operative time (min)	263	603	411	480	428	**unilateral: 337, bilateral: 504**
Flap ischemia time (min)	50	81 (right) 50 (left)	70	50 (right) 50 (left)	61 (right) 36 (left)	**56**
Weight of mastectomy tissue (g)	N/A*	N/A*	N/A*	1250 (right) 1150 (left)	980 (right) 1262 (left)	**1161**
Total abdominal flap weight (g)	1453	1819	1030	2500	1758	**1712**
Breast mound flap weight (g)	767 (left)	850 (right) 794 (left)	555 (left)	1075 (right) 950 (left)	834 (right) 924 (left)	**844**
Function of surgeon	Staff-member	Resident	Staff-member	Resident	Staff-member	
Experience of senior resident (number of DIEP flaps)	N/A*	10 – 20 DIEP flaps	N/A*	>30 DIEP flaps	N/A*	

N/A* = not applicable / not available

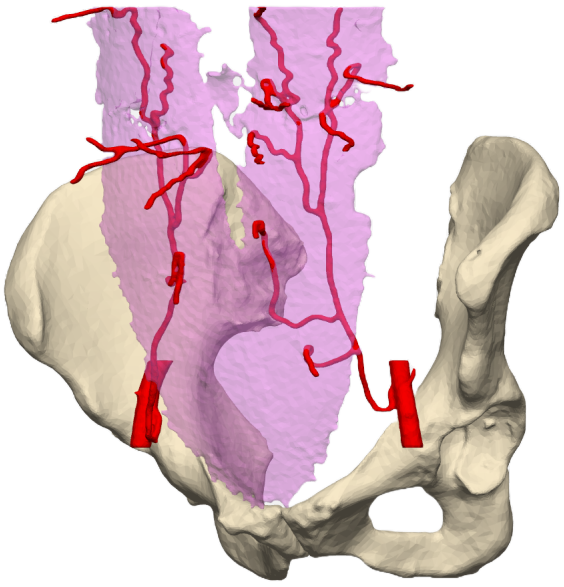

Figure 3.1: Virtual 3D model as seen in Mimics Viewer (Materialise NV, Belgium). The displayed structures are the pelvis, parts of the external iliac arteries, the deep inferior epigastric arteries, its perforators, and the rectus abdominis muscle in transparent setting.

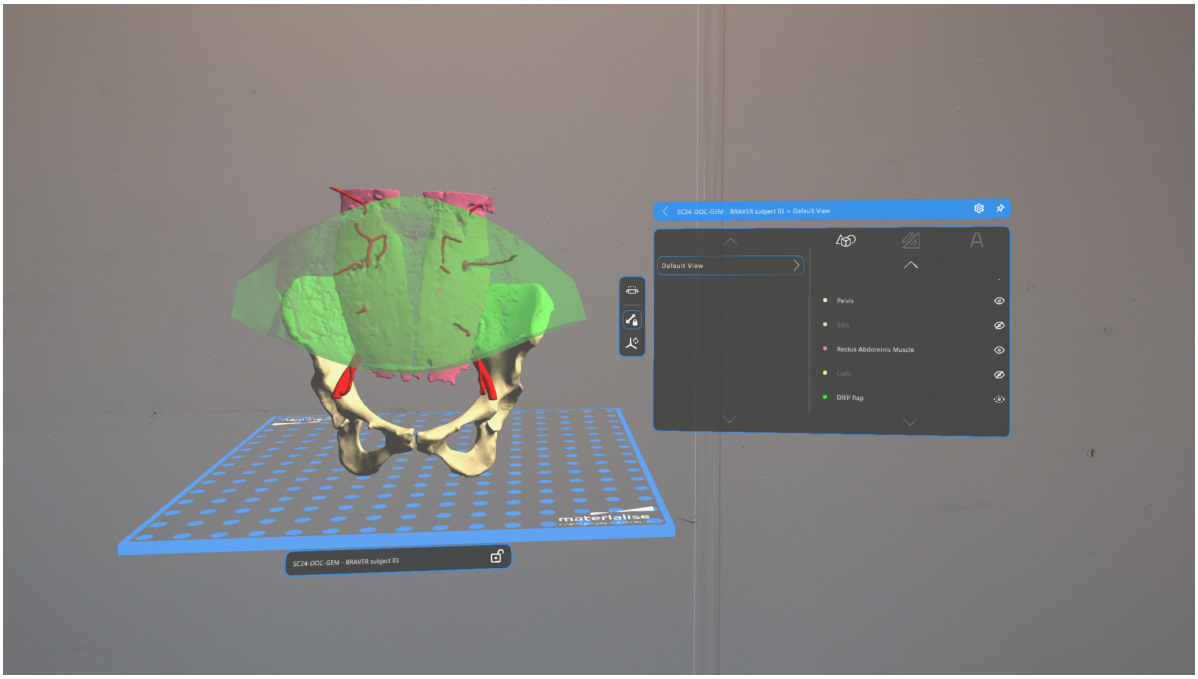

Figure 3.2: XR model as seen through the HoloLens 2 in Mimics Viewer

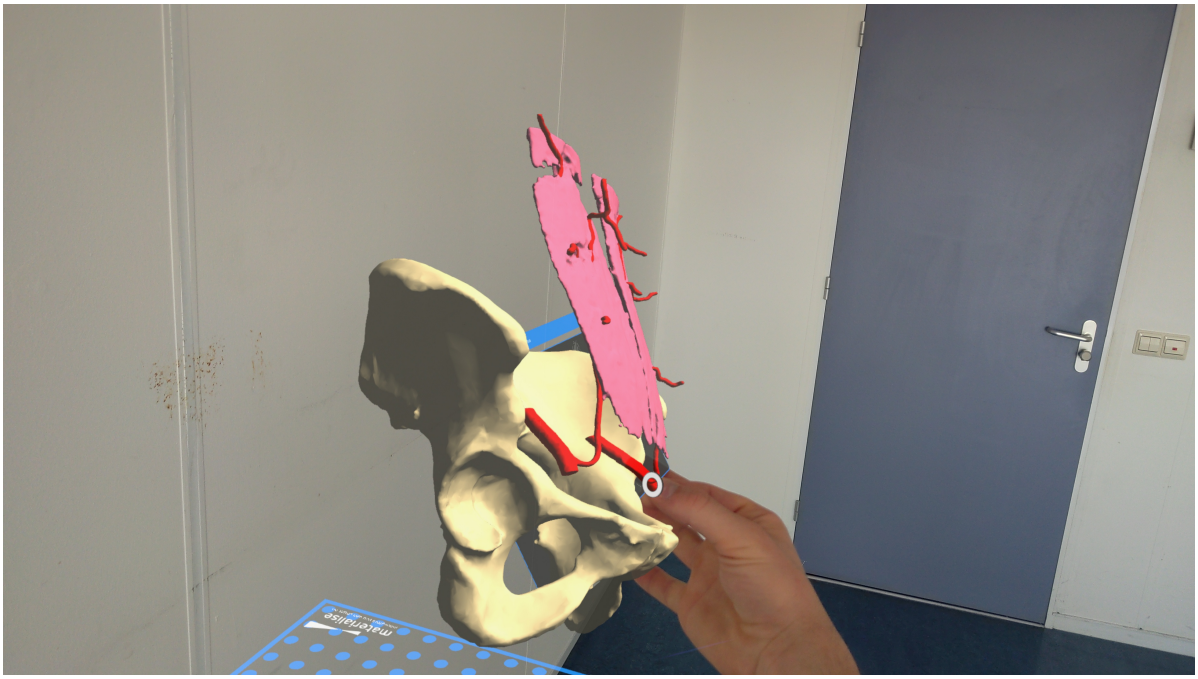

Figure 3.3: Interaction with the virtual 3D model as seen through the HoloLens 2 in Mimics Viewer

3.1.3. Usability score

Immediately after surgery, the participating surgeon was asked to complete the visualization procedures. The SUS was conducted for both CTA and XR. The mean SUS scores were 66 for CTA and 70 for XR. Detailed SUS scores for each item are provided in Table 3.2.

SUS scores of 66 for CTA and 70 for XR fall within the range categorized as 'Good' usability according to the adjective rating scale of Bangor et al. [47]. Figure 3.4 presents a graph illustrating the SUS scores per participant for both CTA and XR, alongside the adjective rating scale.

Table 3.2: System Usability Scale (SUS) outcomes per item

	Item	Mean score CTA	Mean score XR
1	I think that I would like to use this system frequently.	75	80
2	I found the system unnecessarily complex.	80	55
3	I thought the system was easy to use.	70	45
4	I think that I would need the support of a technical person to be able to use this system.	80	75
5	I found the various functions in this system were well integrated.	55	85
6	I thought there was too much inconsistency in this system.	60	75
7	I would imagine that most people would learn to use this system very quickly.	50	85
8	I found the system very cumbersome (meaning awkward) to use.	80	70
9	I felt very confident using the system.	75	60
10	I needed to learn a lot of things before I could get going with this system.	30	65
Mean SUS Score:		**66**	**70**

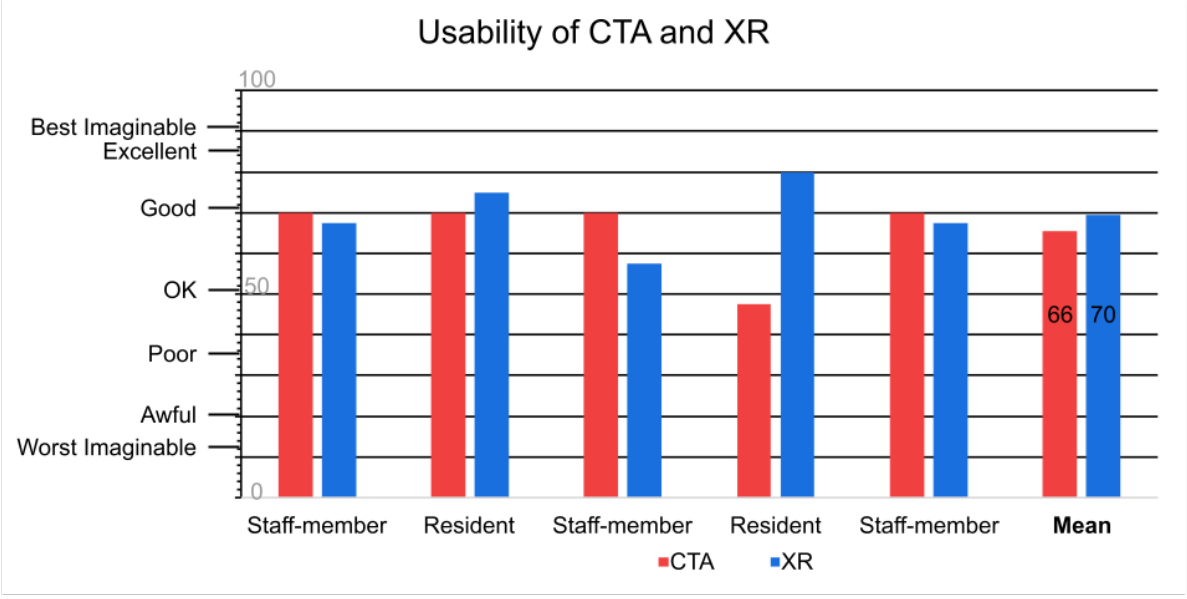

Figure 3.4: Usability score per participant with adjective rating according to Bangor et al. [47]

3.1.4. Perforator characteristics

The questions regarding intraoperative findings of perforator caliber, location within the flap, and intramuscular course as evaluated on CTA and XR yielded the following results.

In terms of caliber, CTA yielded a median score of 3 (mode: 3, range: 2-4), while XR demonstrated a slightly higher median score of 4 (mode: 4, range: 3-5). Regarding the location within the flap, CTA yielded a median score of 4 (mode: 4, range: 3-5), and XR performed slightly higher with a median score of 5 (mode: 5, range: 4-5). Intramuscular course assessment showed equal performance for both CTA and XR, each achieving a median score of 4 (CTA: mode: 4, range: 3-5, XR: mode: 4, range: 3-4).

All results regarding the perforator characteristics are noted in Table 3.3, which provides the median, mode, and range of the perforator characteristics for CTA and XR compared to intraoperative findings. Figure 3.5 illustrates the median scores of perforator characteristics between CTA and XR compared to intraoperative observations.

Table 3.3: Perforator characteristics per visualization method compared to intraoperative findings Scores range from 1 (minimum) to 5 (maximum)

Perforator characteristic		CTA	XR
Location within the flap	Median:	4	5
	Mode:	4	5
	Range:	3-5	4-5
Caliber	Median:	3	4
	Mode:	3	4
	Range:	2-4	3-5
Intramuscular course	Median:	4	4
	Mode:	4	4
	Range:	3-5	3-4

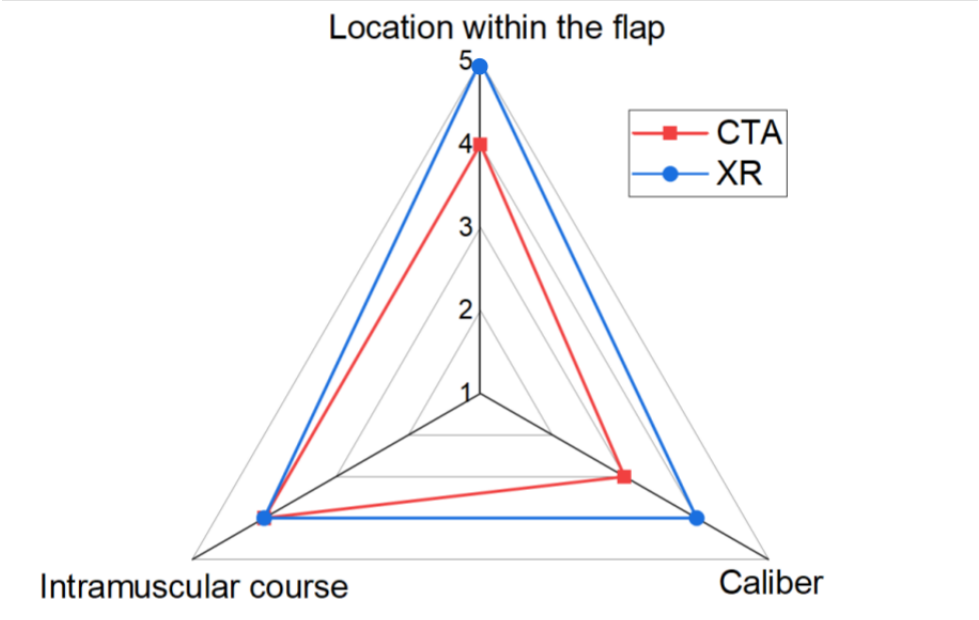

Figure 3.5: Median scores of perforator characteristics per visualization method compared to intraoperative findings. Scores range from 1 (minimum) to 5 (maximum).

3.1.5. Value of XR in addition to CTA

The median score for using XR personally was 4 (mode: 5, range: 2 to 5), and the mean score for recommending XR to a colleague was also 4 (mode: 4, range: 4 to 5). All data regarding the outcomes of the questionnaires can be found in Appendix C.

Out of all responses, only one was negative about XR for preoperative planning, and one was neutral. Figure 3.6 illustrates the results from the last two questions regarding the potential added value of XR in addition to CTA for preoperative planning of DIEP flap BR.

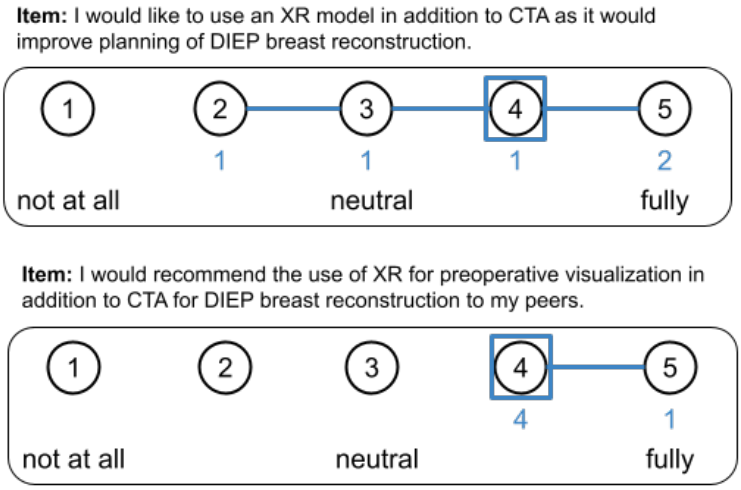

Figure 3.6: Added value of XR in addition to CTA. Scores range from 1 (minimum) to 5 (maximum). The blue square indicates the median score, the blue lines show the range of results, and the blue numbers denote the frequency of each score.

3.2. DIEP flap weight

The following results were obtained from the surgery report, the virtual 3D model of the DIEP flap, and the 2D method described by Nanidis et al. [14]. Figure 3.7 is a screenshot from Mimics 26.0 (Materialise NV, Belgium) where the virtual 3D model of the DIEP flap, the reference points, and the contours of the flap within the CTA images are shown.

The mean difference between true and estimated weight from the virtual 3D model was 333 grams (range: 127– 869). The mean percentage difference was 18.9% (range: 7.0-34.8).

The mean difference between true and estimated weight from the 2D method was 775 grams (range: 178–1298). The mean percentage difference was 44.5% (range: 12,2-60.1). Tables 3.4 and 3.5 contain more detailed information regarding the estimated and true total abdominal flap weight based on the virtual 3D model and 2D method. All individual measurements regarding the 2D method can be found in Appendix C.

Table 3.4: Estimated and true total abdominal flap weight based on the virtual 3D model

Participant	Estimated weight 3D model (g)	True weight (g)	Difference (g)	Percentage difference (%)
1	1691	1453	238	16.4
2	1692	1819	127	7.0
3	1325	1030	295	28.6
4	1631	2500	869	34.8
5	1621	1758	137	7.8
Mean	**1592**	**1712**	**333**	**18.9**

Table 3.5: Estimated and true total abdominal flap weight based on the 2D method

Participant	Estimated weight 2D method (g)	True weight (g)	Difference (g)	Percentage difference (%)
1	1275	1453	178	12.2
2	725	1819	1094	60.1
3	434	1030	596	57.8
4	1202	2500	1298	51.9
5	1047	1758	711	40.4
Mean	**937**	**1712**	**775**	**44.5**

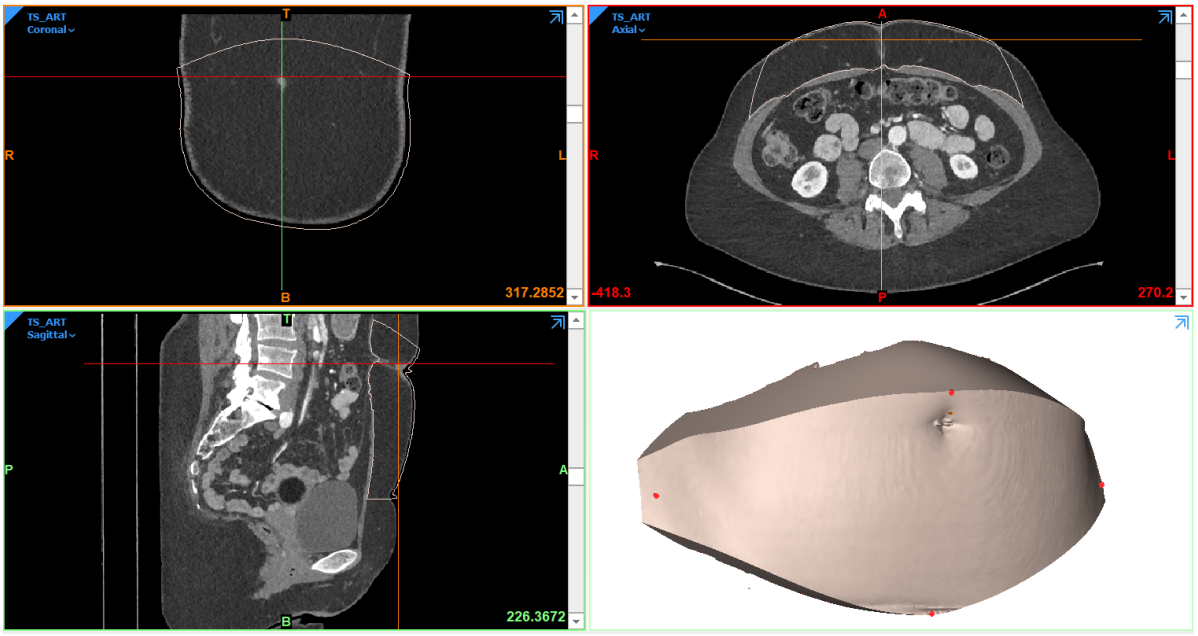

Figure 3.7: Virtual 3D model of a DIEP flap created in Mimics 26.0 (Materialise NV, Belgium). Contours of the DIEP flap are shown in all planar views of the CTA.

4

Discussion

4.1. Usability

DIEP flap BR is the gold standard for ABR following mastectomy. However, it is also challenging and time-consuming, which increases the risk of perioperative complications. As a result, surgeons continually seek methods to enhance this surgical technique to reduce operative times and minimize complications. Various pilot studies have indicated the potential added value of using XR for DIEP flap BR, particularly in reducing operative time and improving perforator identification [29, 35–42].

This pilot study aimed to provide insight into the usability and potential added value, as experienced by the surgeons, of XR in DIEP flap BR to enhance the understanding of the DIEA and its perforators.

This study found that the usability of XR for DIEP flap BR can be categorized as 'Good' and is comparable to CTA. XR showed a slight advantage in the visualization of perforator caliber and location within the flap compared to CTA. The positive feedback from participating surgeons regarding the recommendation of XR to colleagues highlights its potential to enhance surgical planning.

To put the results regarding the usability of this pilot study into perspective, Berger et al. conducted an experiment using the Magic Leap (Magic Leap Inc., Florida, USA) AR-glasses and aligned the MR-A images onto the patient [41]. This study reported a System Usability Scale (SUS) score of 67 (SD: 10), which is comparable to the usability results of XR in this study.

In her master thesis, Kos asked surgeons to choose the dominant perforator for DIEP flap BR using three different viewing modalities: CTA, VR, and a virtual 3D environment displayed on a standard monitor [48]. She then administered the Usefulness, Satisfaction, and Ease of Use (USE) questionnaire to assess the three viewing modalities. Unlike the present study, Kos found that CTA was rated higher in both 'usefulness' and 'ease of use' compared to VR. Another finding of this study was 90% of the participants believed VR would improve preoperative planning when asked in a simple 'Yes' or 'No' format. This finding aligns with the current study, where surgeons expressed a positive attitude for using XR in addition to CTA and indicated they would recommend XR to their colleagues.

In another study, Freidin et al. compared VR to conventional CTA images for evaluating the abdominal vascular anatomy for ABR using a questionnaire created by the authors [29]. Surgeons ranked VR higher than CTA in terms of better anatomical understanding and intraoperative comparability. Furthermore, 86.21% of the surgeons expressed a strong interest in using VR for future planning of abdominal ABR [29]. Another interesting finding from this study was that in four out of forty flaps (10%), surgeons altered their initial surgical plan based on CTA after visualization using VR. Two of the forty planned DIEP procedures were switched to free TRAM, and both initial free TRAM procedures were switched to DIEP flap BR.

The interpretation of individual SUS items should be approached with caution. The creator of the SUS, J. Brooke, emphasizes in his article that "scores for individual items are not meaningful on their own" [46]. Brooke further elaborates in a subsequent article, noting that individual SUS items are not intended

to have diagnostic value by themselves or to relate to specific features of a system [49]. Despite this, more recent studies suggest that there might be significance in the analysis of individual items, such as perceived complexity (”I found the system unnecessarily complex” - item 2), perceived ease of use (”I thought the system was easy to use” - item 3), perceived consistency (“I thought there was too much inconsistency in this system” - item 6), and perceived learnability (”I would imagine that most people would learn to use this system very quickly” - item 7, and ”I needed to learn a lot of things before I could get going with this system” - item 10) [50, 51].

In this study, several results from individual SUS items are noteworthy. For item 2, the mean scores were 80 for CTA and 55 for XR, potentially indicating that XR is perceived as more complex than CTA. For item 3, the mean scores were 70 for CTA and 45 for XR, suggesting that CTA is perceived as easier to use than XR. For perceived learnability, the mean scores for item 7 and item 10 were 50 and 30 for CTA, and 85 and 65 for XR, respectively. These results may indicate a higher perceived learnability for XR compared to CTA. However, it is important to note that all participants in this study had never used XR in a clinical setting before and even the least experienced resident included in this study was accustomed to using CTA for preoperative planning of DIEP flap BR.

This lack of prior experience with XR should also be taken into account, since there may be a learning curve associated with using XR for DIEP flap BR. Seth et al. identified a learning curve of 30 minutes for first-time users of the HoloLens 2 for DIEP flap BR [40]. In another study, Ioschpe et al. described a ”relatively short” learning curve for DIEP flap BR using VR (Google Glasses) [39]. In this study, the surgeons received only a brief introduction to the controls of the HoloLens 2 and the Mimics Viewer software of approximately 1 minute. Even though the HoloLens 2 and Mimics viewer offer intuitive controls, this limited exposure before asking surgeons to assess the 3D virtual model might have influenced their perceptions and usability scores.

The median scores for perforator caliber and location within the flap showed a slight advantage for XR over CTA. More accurate visualization of perforator characteristics could potentially enhance DIEP flap BR, as the operative success of DIEP flap BR is related to the identification of the most suitable and dominant perforators in terms of laterality, caliber, and intramuscular course using CTA imaging [22, 24–26]. However, it’s worth noting that in this study, the assessment of the intramuscular course yielded comparable scores for both XR and CTA.

Another interesting finding of this pilot study is that the potential gain of XR in addition to CTA for the 3D understanding perforator characteristics appears to be small. Nevertheless, three out of five participants showed interest in incorporating XR in addition to CTA in their preoperative planning for DIEP flap BR, and all participants stated they would recommend using XR to their colleagues. The phrasing of these questions might have influenced their responses, as XR was presented as a supplement to CTA, highlighting only the potential benefits for surgeons. Additionally, the participating surgeons were not specifically informed about the downsides of XR, such as the time required to create the model, software costs, and limitations of the virtual 3D model.

Lastly, this study focused on DIEP flap BR because it is considered the gold standard. However, XR technology can be applied to any type of surgery that utilizes 3D imaging data. For instance, a study by Pratt et al. in 2018 demonstrated the use of the HoloLens to identify perforators in various donor sites for extremity reconstruction, showing that XR could accurately localize perforators in other donor site regions. This indicates the broader potential of XR technology for other types of soft tissue surgery [52].

4.2. DIEP flap weight

This study found a mean percentage difference of 18.9% between estimated flap weight derived from the virtual 3D model and the actual flap weight, with a notable spread ranging from 7.0% to 34.8%. However, when compared with the 2D method by Nanidis et al., an even larger discrepancy was found, with a mean percentage difference of 44.5%, ranging from 12.2% to 60.1% [14].

In the initial research by Nanidis et al. on the 2D method, the percentage difference was 6.4%, a significant contrast to the outcomes of this study employing the same method [14]. It is noteworthy that for every case in this study, the 2D method consistently underestimated the total weight of the DIEP

flap in comparison to the actual weight. Many factors could potentially affect the large discrepancy between the percentage difference of the 2D method in this study and the original article, of which the most likely ones will be discussed.

First, it may be possible that the weight difference could stem from variations in mean flap weight and population demographics between Nanidis et al.'s study and this study. Nanidis et al. reported a mean total flap weight of 625 grams in their prospective cohort, significantly lower than the mean flap weight of 1712 grams observed in this study population. Although the BMI of the participants is not disclosed in the study by Nanidis et al., it is plausible that the BMI of the patients is different from the BMI of the participants in this study. The 2D method might be more suited for patients with lower BMI, where flap weights tend to align more closely with the patient characteristics of the original study by Nanidis et al. [14].

Another factor potentially contributing to the variance in the percentage difference of DIEP flap weight estimation could be the surgeons' preferences. The delineation of the borders of the DIEP flap relies on subjective assessment by the operating surgeon during the harvesting procedure. It is conceivable that the surgeons involved in the study by Nanidis et al. may have favored smaller DIEP flaps compared to the surgeons in this study. As a result, the method described by Nanidis et al. might have been tailored to the outcomes of those surgeons and may not be as applicable when harvesting larger DIEP flaps.

Additionally, as the authors note in their article, there could be a learning curve associated with the accurate application of the measuring method, as the outcomes are very sensitive to the measurements performed. It's plausible that the researcher responsible for measurements in this study may not have had sufficient practice with this method, potentially contributing to the notable percentage error observed.

Finally, clothing worn by all participants included in this study during CTA image acquisition poses another significant consideration for accurate measurements. Especially tight-fitting clothes can distort the distribution of adipose tissue within the field of view on the CTA. It's conceivable that this may impact measurements, particularly concerning the thickness (t) of the DIEP flap.

Compared to other 3D volumetric predictions of DIEP flap weight, a mean weight difference of 333 grams and a mean percentage error of 18.9% between estimated flap weight and true flap weight, as observed in this study, is relatively high. Therefore, the methodology used in this study to estimate DIEP flap weight based on the virtual 3D model lacks accuracy and precision and should not be used in clinical practise.

In a study conducted by Rosson et al., flap weight predictions were accurate within 9% of the actual weight for half of their study population using volumetric 3D models of the DIEP flap [16]. This higher level of accuracy can be attributed to the placement of radiopaque markers by the surgeon along the boundaries of the DIEP flap during CTA image acquisition. This ensured clear visibility of the flap boundaries on the skin during the segmentation process, leading to a more precise representation of the actual marking of the DIEP flap according to the surgical plan compared to the segmentation method employed in this study, as outlined in Appendix A.

Even more impressive results were reported by Eder et al., achieving a prediction accuracy within 0.29 ± 3.0% (range: –8.77-5.67) [15]. This heightened accuracy likely stems from the availability of images depicting the presurgical marking of the borders of the DIEP flap, crafted by the surgeon responsible for the flap harvesting. This method allows for a more precise representation of the actual marking of the DIEP flap according to the surgical plan. In this study, the segmentation method was employed without images of the preoperative markings of the DIEP flap, making precise representation of the actual surgical markings more difficult.

4.3. Limitations

The limitations of this pilot study are multifaceted. First, the results presented are only the preliminary findings from a single center of the larger BRAVER study. To date, only five participants from UMC Utrecht have been included. Five surgeons from two additional academic centers are yet to participate.

Secondly, the presence of the researcher during the completion of the postoperative assessment and

questionnaire could have influenced the participants' responses. However, the researcher's main role was to offer technical assistance with HoloLens if needed, while abstaining from making subjective comments that could potentially influence the responses.

Thirdly, the quality of the virtual XR model was dependent on the skills of the researcher performing the segmentations and the image quality of the CTA. In theory, it is possible that a branch of the DIEA might have been missed during the creation of the virtual model. However, an independent second observer always performed a quality check to assess the segmentations for errors before their use in this study.

Lastly, altering the timing of visualization from postoperative to preoperative may influence how surgeons experience and assess the 3D virtual model using XR. This change aligns with standard clinical practice and could enhance surgical planning and execution. Unlike the traditional approach of reviewing 2D CTA images on a standard monitor, XR introduces a paradigm shift by offering the surgeon their initial encounter with a 3D representation of the patient's anatomy. This transition from 2D to 3D visualization represents a fundamental change in how surgeons perceive and interact with anatomical structures during preoperative planning.

4.4. Future perspectives

Based on the preliminary results of the BRAVER study, finishing this study in the other study sites will provide insight into the usability as experienced by users from multiple academic centers.

Additionally, the broader BRAVER study holds potential for more comprehensive insights. While the preliminary findings are based on the single-center experience with only five participants, the inclusion of five additional surgeons from two more academic centers will enhance the study's robustness. By reaching the target of ten participants, the research will enable the creation of subgroups to assess differences in the usability of XR between staff members and residents. This comparison could potentially be interesting, as residents have less experience in mentally translating 2D CTA images into 3D anatomy.

Furthermore, the semi-automatic segmentation of the CTA was time-consuming, taking about five hours per participant. For virtual 3D models to be integrated into clinical practice, a fully automatic segmentation tool is necessary to significantly cut down on virtual 3D model creation time.

Lastly, future research regarding the usability of XR should aim to quantify the added value in terms of total operative time, flap dissection time, and complications by utilizing larger patient cohorts. It is essential that these studies incorporate preoperative rather than postoperative visualization using XR in addition to CTA to better align with clinical practice and offer a more comprehensive evaluation of XR's impact on surgical planning and outcomes. Additionally, surgeons should perform multiple DIEP flap BR procedures, rather than a single evaluation as in this study, to gain experience with the XR models and reduce the effect of the learning curve associated with XR.

4.5. Conclusion

The preliminary findings suggest that XR using the HoloLens 2 is a promising tool for perforator visualization in DIEP flap BR. The similar SUS scores between XR and CTA visualization indicate that XR is as user-friendly as CTA and well-received by surgeons. Surgeons found XR slightly outperformed CTA for visualizing the perforator caliber and location within the flap and expressed positive attitudes towards integrating XR into preoperative planning and recommending it to colleagues. These findings support the potential for XR to enhance surgical planning for DIEP flap BR.

Regarding DIEP flap weight, the methodology used in this study to estimate DIEP flap weight based on the virtual 3D model lacks accuracy and precision and should not be used in clinical practise. Furthermore, this study highlights notable discrepancies between predictions derived from the virtual 3D model and a 2D method in predicting DIEP flap weight. Factors such as patient demographics, surgical technique variability, and measurement accuracy contribute to these discrepancies.

References

[1] H. Sung, J. Ferlay, and et al. R.L. Siegel. “Global cancer statistics 2020: GLOBOCAN estimates of incidence and mortality worldwide for 36 cancers in 185 countries”. In: *CA Cancer J Clin* 71.3 (2021), pp. 209–249.

[2] T. Zhong, J. Hu, and et al. S. Bagher. “A comparison of psychological response, body image, sexuality, and quality of life between immediate and delayed autologous tissue breast reconstruction: A prospective long-term outcome study”. In: *Plast Reconstr Surg* 138.4 (2016), pp. 772–780.

[3] F.P. Albino et al. “Delayed versus delayed-immediate autologous breast reconstruction: A blinded evaluation of aesthetic outcomes”. In: *Arch Plast Surg* 41.3 (2014), pp. 264–270.

[4] S.K. Ng, R.M. Hare, and et al. R.J. Kuang. “Breast reconstruction post mastectomy: Patient satisfaction and decision making”. In: *Ann Plast Surg* 76.6 (2016), pp. 640–644.

[5] N.M. Toyserkani, M.G. Jørgensen, and et al. S. Tabatabaeifar. “Autologous versus implant-based breast reconstruction: A systematic review and meta-analysis of Breast-Q patient-reported outcomes”. In: *J Plast Reconstr Aesthet Surg* 73.2 (2020), pp. 278–285.

[6] L. Brambilla, P. Parisi, and et al. A. Gatto. “A retrospective comparative analysis of latissimus Dorsi (LD) flap versus thoracodorsal artery perforator (TDAP) flap in total breast reconstruction with implants: A pilot study”. In: *J Reconstr Microsurg* 38.6 (2022), pp. 451–459.

[7] M.M. LoTempio and R.J. Allen. “Breast reconstruction with SGAP and IGAP flaps”. In: *Plast Reconstr Surg* 126.2 (2010), pp. 393–401.

[8] N.M. Pantelides, R.C. Jica, and et al. N.G. Patel. “Unilateral breast reconstruction using double transverse upper gracilis (TUG) flaps”. In: *J Plast Reconstr Aesthet Surg* 75.3 (2022), pp. 1164–1170.

[9] T. Jo, D.N. Jeon, and H.H. Han. “The PAP flap breast reconstruction: A practical option for slim patients”. In: *J Reconstr Microsurg* 38.1 (2022), pp. 27–33.

[10] P.L. Myers, J.A. Nelson, and R.J. Allen Jr. “Alternative flaps in autologous breast reconstruction”. In: *Gland Surg* 10.1 (2021), pp. 444–459.

[11] L. de Weerd et al. “Autologous breast reconstruction with a free lumbar artery perforator flap”. In: *Br J Plast Surg* 56.2 (2003). PMID: 12791371, pp. 180–183.

[12] M.Y. Nahabedian and K. Patel. “Autologous flap breast reconstruction: Surgical algorithm and patient selection”. In: *J Surg Oncol* 113.8 (2016), pp. 865–874.

[13] L.C. Wu et al. “Comparison of donor-site morbidity of SIEA, DIEP, and muscle-sparing TRAM flaps for breast reconstruction”. In: *Plast Reconstr Surg* 122.3 (2008), pp. 702–709.

[14] T.G. Nanidis, H. Ridha, and N. Jallali. “The use of computed tomography for the estimation of DIEP flap weights in breast reconstruction: a simple mathematical formula”. In: *J Plast Reconstr Aesthet Surg* 67.10 (2014), pp. 1352–1356.

[15] M. Eder et al. “Three-dimensional prediction of free-flap volume in autologous breast reconstruction by CT angiography imaging”. In: *Int J Comput Assist Radiol Surg* 9.4 (2014), pp. 541–549.

[16] G.D. Rosson et al. “Three-dimensional computed tomographic angiography to predict weight and volume of deep inferior epigastric artery perforator flap for breast reconstruction: 3D CTA and DIEP Flap Weights”. In: *Microsurgery* 31.7 (2011), pp. 510–516.

[17] H. Kim et al. “Preoperative computed tomographic angiography of both donor and recipient sites for microsurgical breast reconstruction”. In: *Plast Reconstr Surg* 130.1 (2012), 11e–20e.

[18] T.M. Newman et al. “Perforator flap magnetic resonance angiography for reconstructive breast surgery: a review of 25 deep inferior epigastric and gluteal perforator artery flap patients”. In: *J Magn Reson Imaging* 31.5 (2010), pp. 1176–1184.

[19] R.J. Allen and P. Treece. “Deep inferior epigastric perforator flap for breast reconstruction”. In: *Ann Plast Surg* 32.1 (1994), pp. 32–38.

[20] H.K. Moon and G.I. Taylor. “The vascular anatomy of rectus abdominis musculocutaneous flaps based on the deep superior epigastric system”. In: *Plast Reconstr Surg* 82.5 (1988), pp. 815–832.

[21] W.M. Rozen, M.W. Ashton, and D. Grinsell. “The branching pattern of the deep inferior epigastric artery revisited in-vivo: a new classification based on CT angiography”. In: *Clin Anat* 23.1 (2010), pp. 87–92.

[22] A. Malhotra et al. “CT-guided deep inferior epigastric perforator (DIEP) flap localization – better for the patient, the surgeon, and the hospital”. In: *Clin Radiol* 68.2 (2013), pp. 131–138.

[23] S.H. Nelissen et al. “Bulging after DIEP breast reconstruction: New insights concerning rectus diastasis and medial perforator harvest”. In: *Plast Reconstr Surg Glob Open* 11.3 (2023), e4840.

[24] R.G. Wade et al. “Perforator mapping reduces the operative time of DIEP flap breast reconstruction: A systematic review and meta-analysis of preoperative ultrasound, computed tomography and magnetic resonance angiography”. In: *J Plast Reconstr Aesthet Surg* 71.4 (2018), pp. 468–477.

[25] R. Ohkuma, R. Mohan, and et al. P.A. Baltodano. “Abdominally based free flap planning in breast reconstruction with computed tomographic angiography: systematic review and meta-analysis”. In: *Plast Reconstr Surg* 133.3 (2014), pp. 483–494.

[26] T. Teunis et al. “CT-angiography prior to DIEP flap breast reconstruction: a systematic review and meta-analysis”. In: *Microsurgery* 33.6 (2013), pp. 496–502.

[27] J.V. Vasile and J.L. Levine. “Magnetic resonance angiography in perforator flap breast reconstruction”. In: *Gland Surg* 5.2 (2016), pp. 197–211.

[28] D.W. Mathes and P.C. Neligan. “Preoperative imaging techniques for perforator selection in abdomen-based microsurgical breast reconstruction”. In: *Clin Plast Surg* 37.4 (2010), pp. 581–591, xi.

[29] D. Freidin, R. Singolda, and S. Tejman-Yarden. “Using Virtual Reality for Deep Inferior Epigastric Perforator Flap Preoperative Planning”. In: *Plast Reconstr Surg Glob Open* 11.1 (2023), e4773.

[30] T.J. Brigham. “Reality check: Basics of augmented, virtual, and mixed reality”. In: *Med Ref Serv Q* 36.2 (2017), pp. 171–178.

[31] M.D. Vles et al. “Virtual and augmented reality for preoperative planning in plastic surgical procedures: A systematic review”. In: *J Plast Reconstr Aesthet Surg* 73.11 (2020), pp. 1951–1959.

[32] J. Kanevsky et al. “Making augmented and virtual reality work for the plastic surgeon”. In: *Ann Plast Surg* 82.4 (2019), pp. 363–368.

[33] J. Zhang, V. Lu, and V. Khanduja. “The impact of extended reality on surgery: a scoping review”. In: *Int Orthop* 47.3 (2023), pp. 611–621.

[34] C. Andrews et al. “Extended reality in medical practice”. In: *Curr Treat Options Cardiovasc Med* 21.4 (2019), p. 18.

[35] S. Hummelink et al. “Preliminary results using a newly developed projection method to visualize vascular anatomy prior to DIEP flap breast reconstruction”. In: *J Plast Reconstr Aesthet Surg* 68.3 (2015), pp. 390–394.

[36] S. Hummelink et al. “An innovative method of planning and displaying flap volume in DIEP flap breast reconstructions”. In: *J Plast Reconstr Aesthet Surg* 70.7 (2017), pp. 871–875.

[37] S. Hummelink et al. “A new and innovative method of preoperatively planning and projecting vascular anatomy in DIEP flap breast reconstruction: A randomized controlled trial”. In: *Plast Reconstr Surg* 143.6 (2019), 1151e–1158e.

[38] G. Masterton et al. “HoloLens in breast reconstruction: What is the future?” In: *Plast Reconstr Surg* 151.6 (2023), 915e–917e.

[39] I. Via Ioschpe et al. “Preoperative planning using virtual reality and computed tomography angiogram in deep inferior epigastric perforator flap breast reconstruction”. In: *J Plast Reconstr Aesthet Surg* 87 (2023), pp. 161–169.

[40] I. Seth, J. Lindhardt, and et al. A. Jakobsen. “Improving visualization of intramuscular perforator course: Augmented reality headsets for DIEP flap breast reconstruction”. In: *Plast Reconstr Surg Glob Open* 11.9 (2023), e5282.

[41] M.F. Berger, R. Winter, and et al. A.-C. Tuca. “Workflow assessment of an augmented reality application for planning of perforator flaps in plastic reconstructive surgery: Game or game changer?” In: *Digit Health* 9 (2023), p. 20552076231173554.

[42] D.J. Cholok et al. “Spatial Fidelity of Microvascular Perforating Vessels as Perceived by Augmented Reality Virtual Projections”. In: *Plast Reconstr Surg* 153 (2024), pp. 524–534.

[43] J. Nielsen and R. Molich. “How to Conduct a Heuristic Evaluation”. In: *Heuristic evaluation*. 1990.

[44] J. Nielsen. *Why you only need to test with 5 users*. 2000. URL: `https://www.nngroup.com/articles/why-you-only-need-to-test-with-5-users/` (visited on 05/24/2024).

[45] J. Sauro. *10 things to know about the system usability scale (SUS)*. 2024. URL: `https://measuringu.com/10-things-sus/` (visited on 05/24/2024).

[46] J. Brooke. “SUS: A quick and dirty usability scale”. In: *Usability Eval Ind*. 1995, p. 189.

[47] A. Bangor, P. Kortum, and J. Miller. “Determining what individual SUS scores mean: adding an adjective rating scale”. In: *J Usability Stud* 4 (2009), pp. 114–123.

[48] T.M. Kos. “Extended Reality for Preoperative Planning of Autologous Breast Reconstructions”. 2022.

[49] J. Brooke. “SUS: A Retrospective”. In: *Journal of Usability Studies* 8.2 (2013), pp. 29–40.

[50] J.R. Lewis and J. Sauro. “Item Benchmarks for the System Usability Scale”. In: *Journal of Usability Studies* 13.3 (May 2018), pp. 158–167.

[51] J.R. Lewis. “The system usability scale: Past, present, and future”. In: *Int J Hum Comput Interact* 34.7 (2018), pp. 577–590.

[52] P. Pratt, M. Ives, and et al. G. Lawton. “Through the HoloLens™looking glass: augmented reality for extremity reconstruction surgery using 3D vascular models with perforating vessels”. In: *Eur Radiol Exp* 2.1 (2018), p. 2.

A

BRAVER Questionnaire

Introduction

Thank you for participating in this study. The goal of this qualitative questionnaire is to assess the usability of XR for perforator visualisation in DIEP breast reconstruction.

Participant characteristics

1. My function is: *
    - O Staff-member
    - O Resident (AIOS)
2. Participated in ... DIEP breast reconstructions
    - O 0 - 10
    - O 10 - 20
    - O 20 - 30
    - O > 30

Ensure the surgeon has assessed the CTA before the questionnaire is continued

System Usability Scale CTA

System Usability Scale (SUS): (Likert scoring: 1 = strongly disagree, 5 = strongly agree)

1. I think that I would like to use this system frequently. *
    - O 1 = strongly disagree
    - O 2
    - O 3 = neutral
    - O 4
    - O 5 = strongly agree
2. I found the system unnecessarily complex. *
    - O 1 = strongly disagree
    - O 2
    - O 3 = neutral
    - O 4
    - O 5 = strongly agree

3. I thought the system was easy to use. *
    - O 1 = strongly disagree
    - O 2
    - O 3 = neutral
    - O 4
    - O 5 = strongly agree
4. I think that I would need the support of a technical person to be able to use this system. *
    - O 1 = strongly disagree
    - O 2
    - O 3 = neutral
    - O 4
    - O 5 = strongly agree
5. I found the various functions in this system were well integrated. *
    - O 1 = strongly disagree
    - O 2
    - O 3 = neutral
    - O 4
    - O 5 = strongly agree
6. I thought there was too much inconsistency in this system. *
    - O 1 = strongly disagree
    - O 2
    - O 3 = neutral
    - O 4
    - O 5 = strongly agree
7. I would imagine that most people would learn to use this system very quickly. *
    - O 1 = strongly disagree
    - O 2
    - O 3 = neutral
    - O 4
    - O 5 = strongly agree
8. I found the system very cumbersome (meaning awkward) to use. *
    - O 1 = strongly disagree
    - O 2
    - O 3 = neutral
    - O 4
    - O 5 = strongly agree
9. I felt very confident using the system. *
    - O 1 = strongly disagree
    - O 2
    - O 3 = neutral
    - O 4

- O 5 = strongly agree

10. I needed to learn a lot of things before I could get going with this system *
    - O 1 = strongly disagree
    - O 2
    - O 3 = neutral
    - O 4
    - O 5 = strongly agree

Additional questions CTA

Additional Questions regarding spatial orientation based on CTA scan: (Likert scoring: 1 = Not at all, 5 = Fully)

CTA provided a good understanding of the following perforator characteristics compared to intraoperative findings:

1. Location in the flap *
    - O 1 = not at all
    - O 2
    - O 3 = neutral
    - O 4
    - O 5 = fully
2. Caliber *
    - O 1 = not at all
    - O 2
    - O 3 = neutral
    - O 4
    - O 5 = fully
3. Intramuscular course *
    - O 1 = not at all
    - O 2
    - O 3 = neutral
    - O 4
    - O 5 = fully
4. CTA provided an overall accurate representation of the anatomy as observed during surgery. *
    - O Yes
    - O No

Ensure the surgeon has assessed the XR model before the questionnaire is continued

System Usability Scale XR

System Usability Scale (SUS): (Likert scoring: 1 = strongly disagree, 5 = strongly agree)

1. I think that I would like to use this system frequently. *
    - O 1 = strongly disagree
    - O 2
    - O 3 = neutral

- O 4
- O 5 = strongly agree

2. I found the system unnecessarily complex. *
   - O 1 = strongly disagree
   - O 2
   - O 3 = neutral
   - O 4
   - O 5 = strongly agree
3. I thought the system was easy to use. *
   - O 1 = strongly disagree
   - O 2
   - O 3 = neutral
   - O 4
   - O 5 = strongly agree
4. I think that I would need the support of a technical person to be able to use this system. *
   - O 1 = strongly disagree
   - O 2
   - O 3 = neutral
   - O 4
   - O 5 = strongly agree
5. I found the various functions in this system were well integrated. *
   - O 1 = strongly disagree
   - O 2
   - O 3 = neutral
   - O 4
   - O 5 = strongly agree
6. I thought there was too much inconsistency in this system. *
   - O 1 = strongly disagree
   - O 2
   - O 3 = neutral
   - O 4
   - O 5 = strongly agree
7. I would imagine that most people would learn to use this system very quickly. *
   - O 1 = strongly disagree
   - O 2
   - O 3 = neutral
   - O 4
   - O 5 = strongly agree
8. I found the system very cumbersome (meaning awkward) to use. *
   - O 1 = strongly disagree
   - O 2

- O 3 = neutral
- O 4
- O 5 = strongly agree

9. I felt very confident using the system. *
   - O 1 = strongly disagree
   - O 2
   - O 3 = neutral
   - O 4
   - O 5 = strongly agree
10. I needed to learn a lot of things before I could get going with this system *
    - O 1 = strongly disagree
    - O 2
    - O 3 = neutral
    - O 4
    - O 5 = strongly agree

Additional questions XR

Additional Questions regarding spatial orientation based on XR scan: (Likert scoring: 1 = Not at all, 5 = Fully)

XR provided a good understanding of the following perforator characteristics compared to intraoperative findings:

1. Location in the flap *
   - O 1 = not at all
   - O 2
   - O 3 = neutral
   - O 4
   - O 5 = fully
2. Caliber *
   - O 1 = not at all
   - O 2
   - O 3 = neutral
   - O 4
   - O 5 = fully
3. Intramuscular course *
   - O 1 = not at all
   - O 2
   - O 3 = neutral
   - O 4
   - O 5 = fully
4. XR provided an overall accurate representation of the anatomy as observed during surgery. *
   - O Yes
   - O No

Added value of XR

Final questions regarding the additional value of XR: (Likert scoring: 1 = Not at all, 5 = Fully)

1. I would like to use an XR model in addition to CTA as it would improve planning of DIEP breast reconstruction. *
    - O 1 = not at all
    - O 2
    - O 3 = neutral
    - O 4
    - O 5 = fully
2. I would recommend the use of XR for preoperative visualisation in addition to CTA for DIEP breast reconstruction to my peers. *
    - O 1 = not at all
    - O 2
    - O 3 = neutral
    - O 4
    - O 5 = fully
3. This is a box for your remarks. Please write anything that comes to mind regarding this study *

End of the questionnaire

You have now reached the end of the questionnaire. Thank you for participating in this study!

B

Segmentation Protocol

Semi-Automatic Perforator Segmentation of abdominal CTA images using Mimics 26.0

Versions:
Document drafted on March. 20, 2024, by K. Zijlstra
Version 2.0 drafted on April. 5, 2024, by K. Zijlstra

Requirements

1. Materialise Mimics version 26.0
2. Materialise 3-matic 18.0
3. Materialise Mimics Viewer Version 2.2.43.9
4. Abdominal CTA scan (slice thickness < 1.0 mm)

Import scan

1. Import the CTA scan by going to “File” and select “New Project”

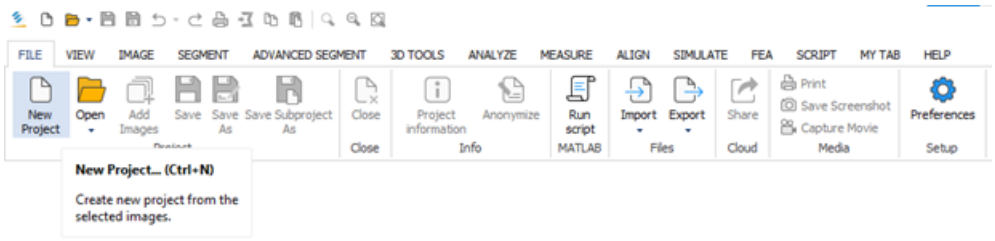

2. Select the scan in the axial plane. If multiple scans in the axial plane exist, choose the scan in the late arterial phase.
3. Go to the object window and create the following group folders:
   (a) Pelvis and large arteries
   (b) Skin
   (c) Muscle
   (d) Subcutaneous fat
   (e) DIEA and perforators
   (f) SIEA
   (g) DIEP flap
   (h) Final parts

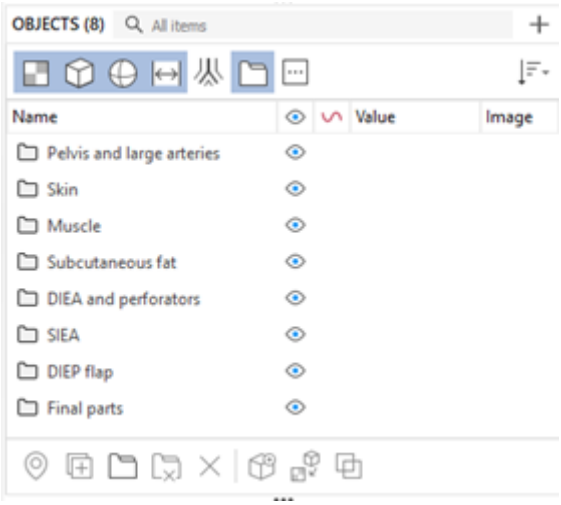

4. If necessary, adjust the contrast by holding the right mouse button and shifting the mouse key in one of the planar views.

Pelvis and large arteries

5. Open the folder “Pelvis and large arteries” in the object window
6. Go to ”SEGMENT” and choose “New Mask”. Select the predefined threshold of
7. To split the mask, go to ”Split Mask” Select the mask “Bones and Contrast Agent”, rename “Region A” ”Pelvis_mask” and “Region B” “Contrast Agent”. Add a new region and name this region “Other Bone”. Carefully use the brush in all three planes to split the mask into arteries, pelvis (without the sacral part), and other bones consisting of the femur, sacrum and lumbar spine. Then, click “OK”.
8. Create two duplicates from “Constrast Agent” and store these duplicates in the folders “DIEA and perforators” and “SIEA”.
9. To isolate the pelvis, go to ”SEGMENT” and choose “Region Grow”. Select the mask ”Pelvis_mask” as “Source” and “<New Mask>” as“Target”. Next, Click on the right and left parts of the pelvis in any of the three planar views. Name this resultis mask “Pelvis_Mask” and delete the older version of “Pevlis_Mask”.
10. To fill in the hollow parts of the pelvis go to ”SEGMENT” and “Smart fill”. Select the mask “Skin and Subcutaneous fat”, set “Hole Closing Distance” to 2 voxels and click “Fill Holes”. Inspect if the skin and fat layer are connected by new green colored voxels. Then, click “OK”.
11. Create a part from the mask “Pelvis_mask” by going to ”SEGMENT” and select “Part”. Select the mask “Pelvis_mask”. Set “Quality” to “Optimal*”. customize the settings to:
    (a) Smoothing ‘on’: 2 iterations 0.3 smooth factor.
    (b) Triangle reduction ‘on’.
12. Rename the newly created part “Pelvis_part”.
13. Next, go to “3D TOOLS” and select the “Wrap” function. Select the part
    (a) Smallest detail = 0.6 – 1 mm (≤slice thickness)
    (b) Gap closing distance = 0.6 – 1 mm (≤slice thickness)
14. Rename the newly created part “Pelvis”
15. Create two duplicates from “Pelvis” and store these parts in the folders “DIEP flap” and “Final parts”.

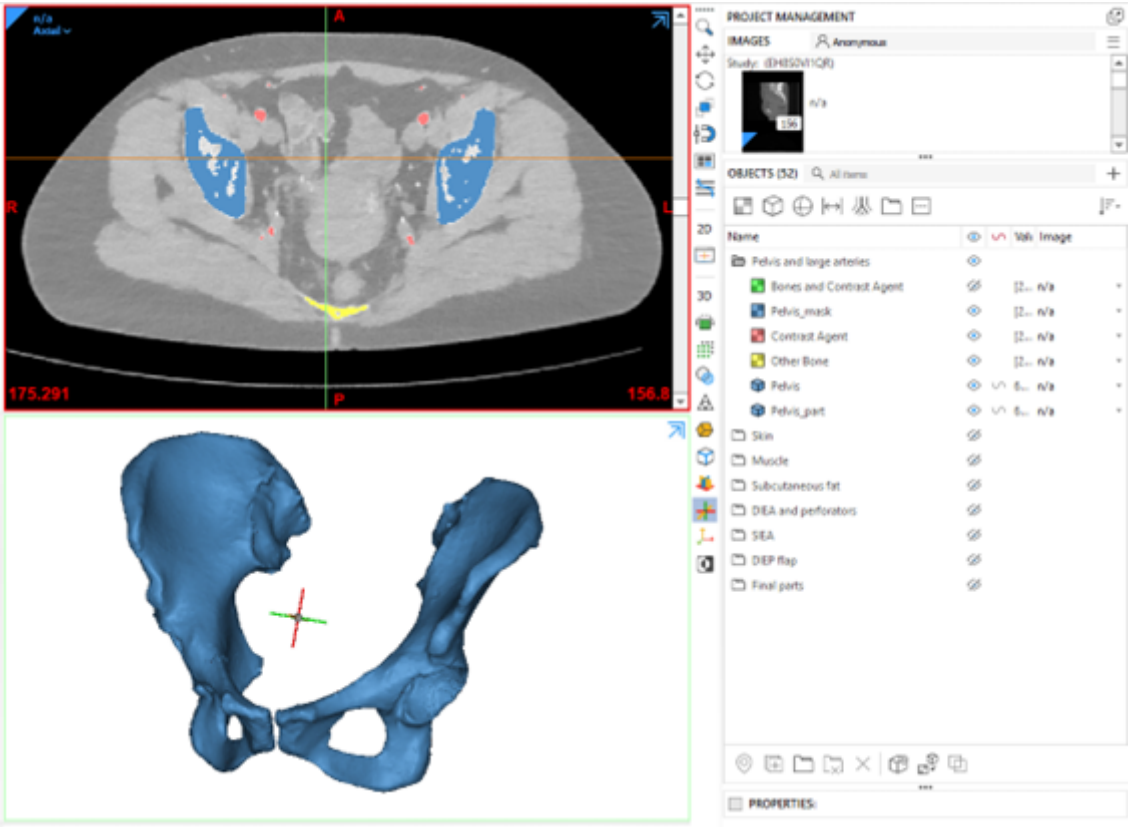

Skin

16. Open the folder “Skin” in the object window
17. Go to ”SEGMENT” and choose “New Mask”. Select the predefined threshold of “Skin Tissue (CT, Adult)” and select OK. Name this mask “Skin_mask”.
18. To isolate the (anterior) skin layer, go to ”SEGMENT” and choose “Region Grow”. Select the mask “Skin_mask” for both “Source” and “Target”. Next, Click on the anterior part of the skin in any of the three planar views.
19. Create a duplicate from “Skin_mask” and safe this duplicate in the folder “Subcutaneous fat”.
20. Create a part from the mask “Skin_mask” by going to ”SEGMENT” and select “Part”. Select the mask “Skin_mask”. Set “Quality” to “Optimal*”. customize the settings to:
    (a) Smoothing ‘on’: 2 iterations 0.3 smooth factor.
    (b) Triangle reduction ‘on’.
21. Rename the newly created part “Skin_part”.
22. Next, go to “3D TOOLS” and select the “Wrap” function. Select the part “Skin_part” and use the following settings:
    (a) Smallest detail = 0.6 – 1 mm (≤slice thickness)
    (b) Gap closing distance = 0.6 – 1 mm (≤slice thickness)
23. Rename the newly created part “Skin”
24. Create a duplicate from “Skin” Open the folder and store this part in the folder “Final parts”.

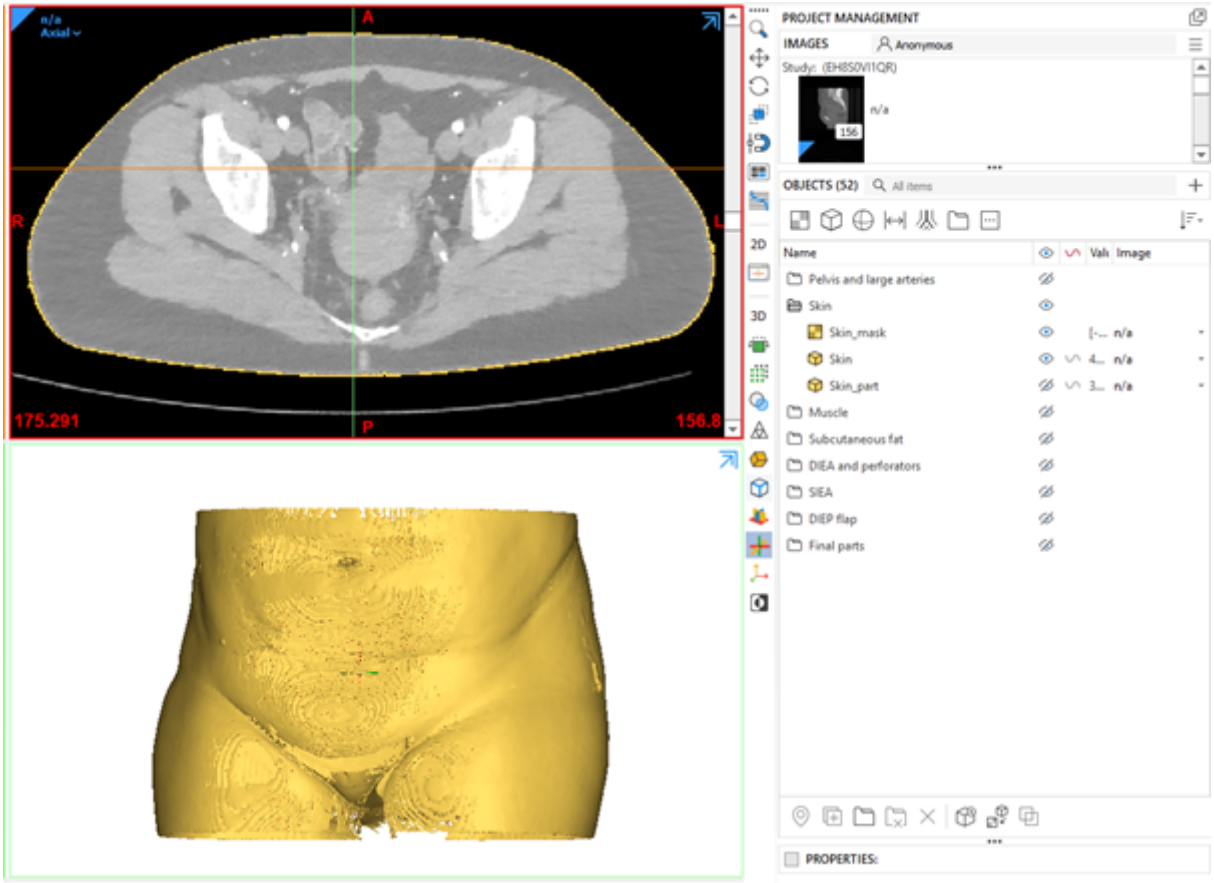

Muscle

25. Open the folder “Muscle” in the object window
26. Go to ”SEGMENT” and choose “New Mask”. Select the predefined threshold of “Muscle Tissue (CT, Adult)” and select OK. Name this mask “Muscles”.
27. To split the mask, go to ”Split Mask” Select the mask “Muscles”, rename “Region A” “Rectus Abdominis Muscle_mask” and “Region B” “Other Muscle”. Carefully use the brush in all three planes to split the mask into the rectus abdominis muscle and other muscles. Note that other parts of the CTA, such as the filled colon, can have similar Hounsfield values that are within the muscle threshold. Carefully segment these parts using the “Split Mask” function in the mask “Other Muscle”. Then, click “OK”.
28. To isolate the rectus muscle, go to ”SEGMENT” and choose “Region Grow”. Select the mask “Rectus Abdominis Muscle_mask” for both “Source” and “Target”. Next, Click on the rectus muscle in any of the three planar views.
29. Create a part from the mask “Rectus Abdominis Muscle_mask by going to ”SEGMENT” and select “Part”. Select the mask “Rectus Abdominis Muscle_mask”. Set “Quality” to “Optimal*”. customize the settings to:
    (a) Smoothing ‘on’: 2 iterations 0.3 smooth factor.
    (b) Triangle reduction ‘on’.
30. Rename the newly created part “Rectus Abdominis Muscle_part”.
31. Next, go to “3D TOOLS” and select the “Wrap” function. Select the part “Rectus Abdominis Muscle_part” and use the following settings:
    (a) Smallest detail = 0.6 – 1 mm (≤slice thickness)
    (b) Gap closing distance = 0.6 – 1 mm (≤slice thickness)
32. Rename the newly created part “Rectus Abdominis Muscle”
33. Create a duplicate from “Rectus Abdominis Muscle” Open the folder and store this part in the folder “Final parts”.

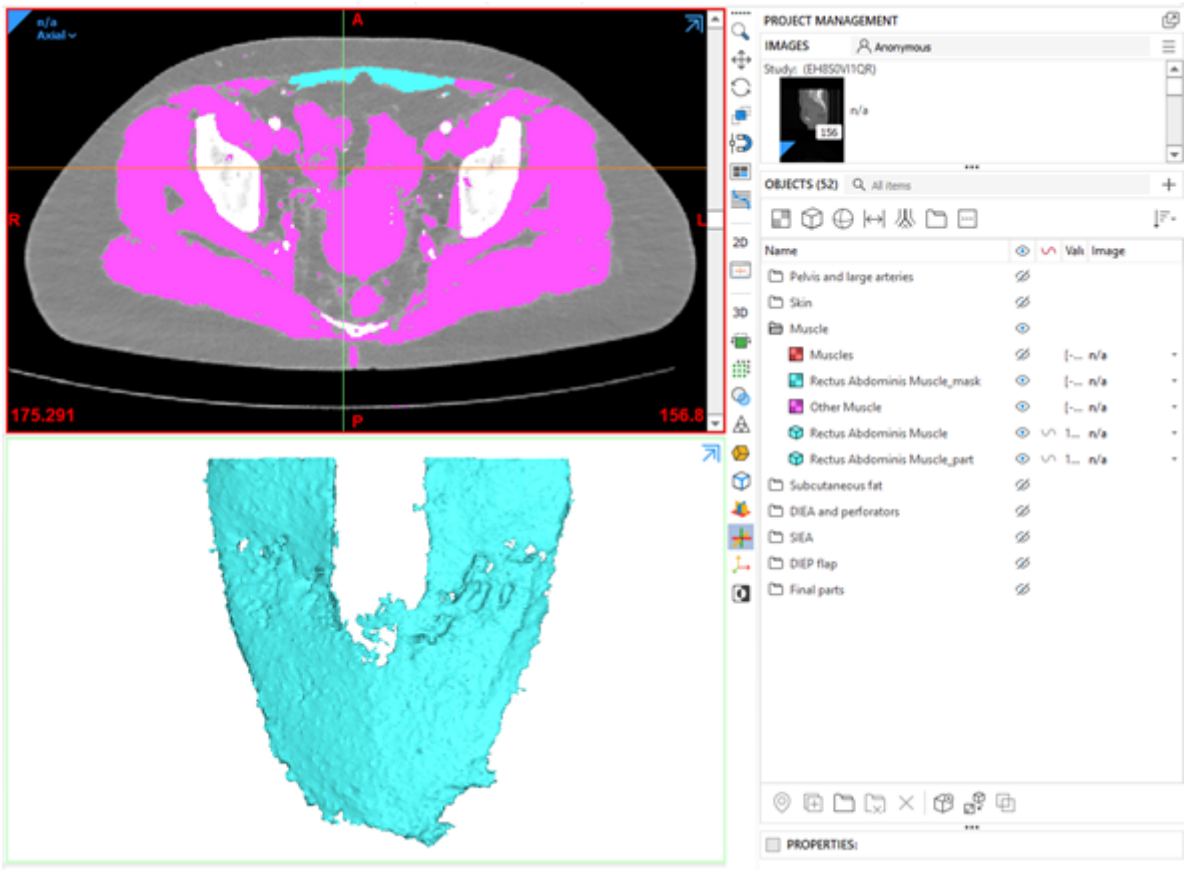

Subcutaneous fat

34. Open the folder “Subcutaneous fat” in the object window
35. Go to ”SEGMENT” and choose “New Mask”. Select the predefined threshold of “Fat Tissue (CT, Adult)” and select OK. Name this mask “Fat”.
36. To split the mask, go to ”Split Mask” Select the mask “Fat”, rename “Region A” “Subcutaneous fat” and “Region B” “Other fat”. Carefully use the brush in all three planes to split the mask into the Subcutaneous fat and the intra-abdominal fat. Then, click “OK”.
37. Next, merge the masks ”Skin_mask” and “Subcutaneous fat” by going to ”SEGMENT” and go to “Boolean Operations”. Select “Subcutaneous fat” for Mask A and the mask we duplicated earlier and saved in this file “Skin_mask” for Mask B. Set “Operation” to ”Unite” and name the “Target Mask Name” “Skin and Subcutaneous fat”. Then, click “APPLY”
38. To fill in the space between the skin layer and the subcutaneous and fill the holes in the subcutaneous fat go to ”SEGMENT” and “Smart fill”. Select the mask “Skin and Subcutaneous fat”, set “Hole Closing Distance” to 2 voxels and click “Fill Holes”. Inspect if the skin and fat layer are connected by new green colored voxels. Then, click “OK”.
39. Rename the newly created mask “Cutis_mask”.
40. To isolate the cutis, go to ”SEGMENT” and choose “Region Grow”. Select the mask “Cutis_mask” for both “Source” and “Target”. Next, Click on the subcutaneous fat in any of the three planar views.
41. Create a part from the mask “Cutis_mask” by going to ”SEGMENT” and select “Part”. Select the mask “Cutis_mask”. Set “Quality” to “Optimal*”. customize the settings to:
    (a) Smoothing ‘on’: 2 iterations 0.3 smooth factor.
    (b) Triangle reduction ‘on’.
42. Rename the newly created part “Cutis_part”.
43. Next, go to “3D TOOLS” and select the “Wrap” function. Select the part “Rectus Abdominis Cutis_part” and use the following settings:
    (a) Smallest detail = 0.6 – 1 mm (≤slice thickness)
    (b) Gap closing distance = 0.6 – 1 mm (≤slice thickness)
44. Rename the newly created part “Cutis”
45. Create two duplicates from “Cutis” and save one part in the folder “Final parts” and the other in the folder “DIEP flap”.

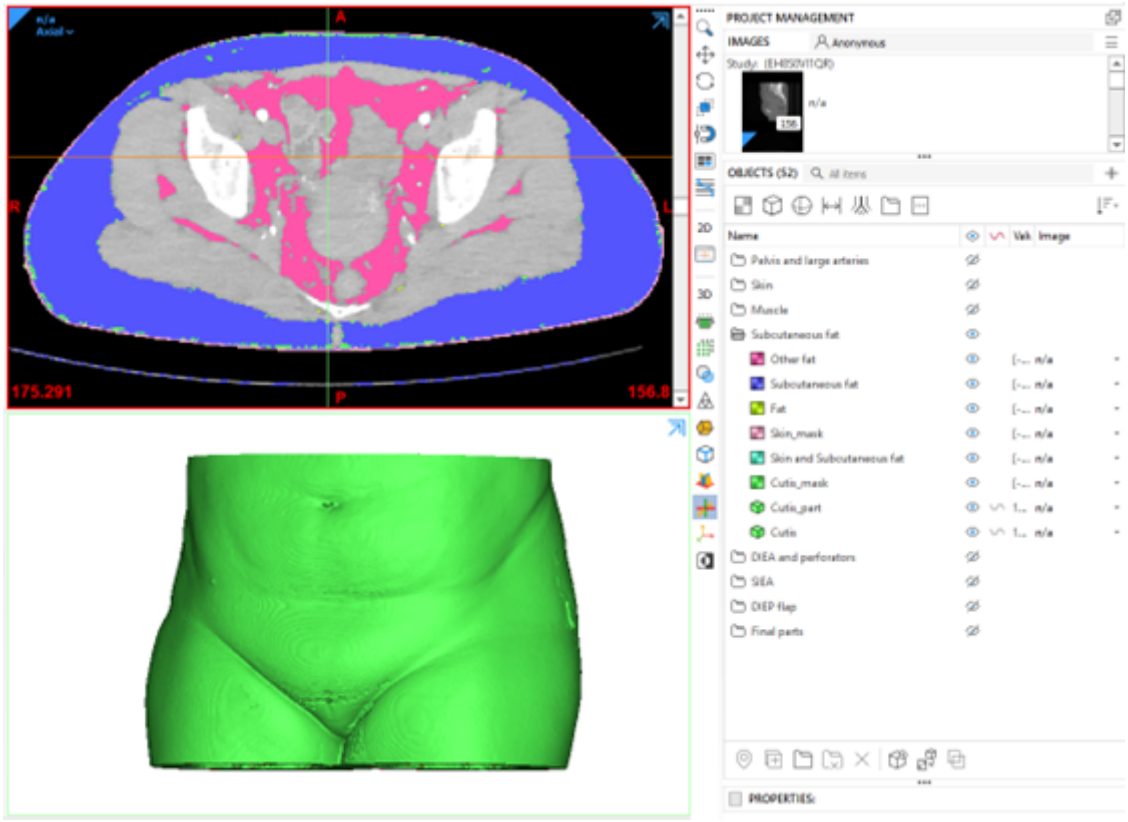

DIEA and perforators

46. Open the folder “DIEA and perforators” in the object window
47. Select the previously stored mask “Contrast Agent” and go to ”SEGMENT” and “Edit Mask”. Select the operation “Remove” and options “Elipse”. Search in the Axial plane to the branching of the left DIEA. Remove a few slices around 2 centimeters both cranial and caudal of the external iliac artery both cranial and caudal from the branching of the DIEA.
48. Go to ”SEGMENT” and select “Region Grow”. Select “Contrast Agent” as the source mask and as target mask “<New Mask>”. Click on the right and left DIEA as previously cut off from the other parts of the mask “Contrast Agent”. Name this resulting mask “Left External Iliac Artery”.
49. Go to ”SEGMENT” and click on “Thin Structure”. Search for the origin of the deep inferior epigastric artery (DIEA) of the left side in any of the three planar views and click on the origin. From there, continue the path of the DIEA in any of the three planar views (you can continue in any planar view where the pathway of the left DIEA is the clearest. Rename the created structures in a logical way such as: “Left DIEA part 1”
50. For any branching of the DIEA, repeat the step above. Later on, we can merge these multiple parts.
51. Next, go to “Mask from Object”. And merge the different parts of the DIEA and DIEP(s) together in a new mask. Rename this mask “left DIEA and perforators”
52. Go to “Segement” and select “Boolean Operations”. Select “left DIEA and perforators” as Mask A and “Left External Iliac Atery” as Mask B. Select “Unite” for operations and name the resulting mask “left DIEP”
53. It is important to assess the newly created mask of the DIEA and its perforators in all three planar views. If necessary, adjust the mask with the “Edit Mask” tool.
54. Create a part from the mask “left DIEP” by going to ”SEGMENT” and select “Part”. Select the mask “left DIEP”. Set “Quality” to “Optimal*”. customize the settings to:
    (a) Smoothing ‘on’: 2 iterations 0.3 smooth factor.
    (b) Triangle reduction ‘on’.
55. Rename the newly created part “left DIEP_part”.
56. Next, go to “3D TOOLS” and select the “Wrap” function. Select the part “left DIEP_part” and use the following settings:
    (a) Smallest detail = 0.6 – 1 mm (≤slice thickness)
    (b) Gap closing distance = 0.6 – 1 mm (≤slice thickness)
57. Rename the newly created part “left DIEP”
58. Create a duplicate from “left DIEP” Open the folder and store this part in the folder “Final parts”.
59. Repeat this chapter for the external iliac artery, the DIEA and the perforators at the right side of the patient.

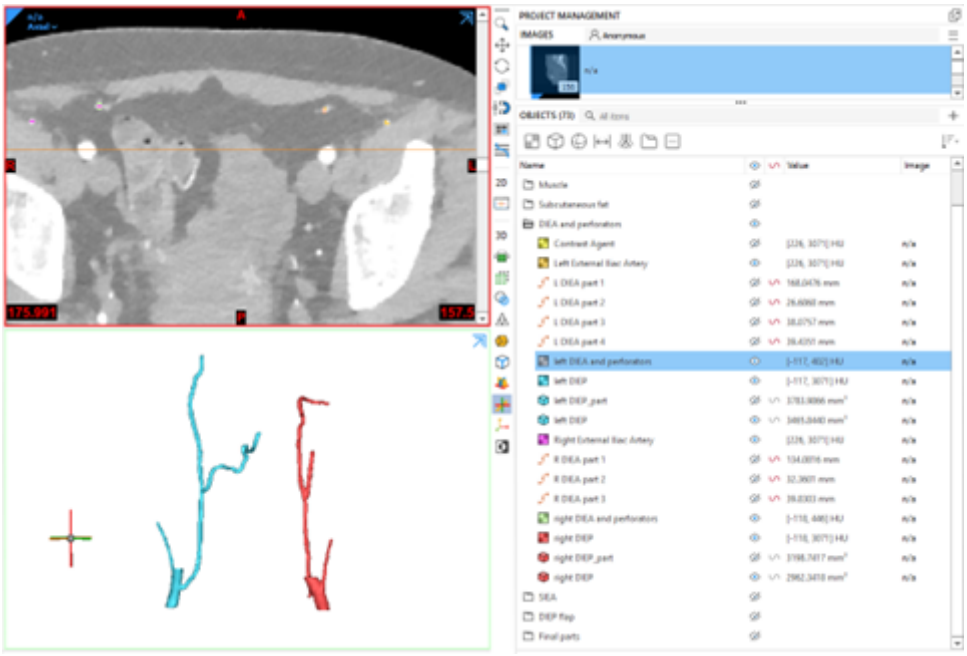

(SIEA)

60. If desired and detectable on the CTA, the same steps for the DIEA and perforators can be repeated to segment the external iliac artery, the superficial epigastric artery (SIEA) and its perforators on both sides of the patient.

DIEP flap

61. Open the folder “DIEA and perforators” in the object window and visualise the parts “Pelvis” and “Cutis”.
62. The next step is to indicate what part of the cutis will become DIEP flap. First, go to “ANALYZE” and select “Point”. Visualise the part “Cutis_part” and place the following four points (also using the “Distance” function that can be found under “MEASURE”):
    (a) Superior point: One centimeter cranial from the center of the Umbilicus at the anterior side of the part “Cutis”
    (b) Inferior Point: Seven centimeter cranial from the introitus (in the natural fold of the skin if applicable) at the anterior side of the part “Cutis”.

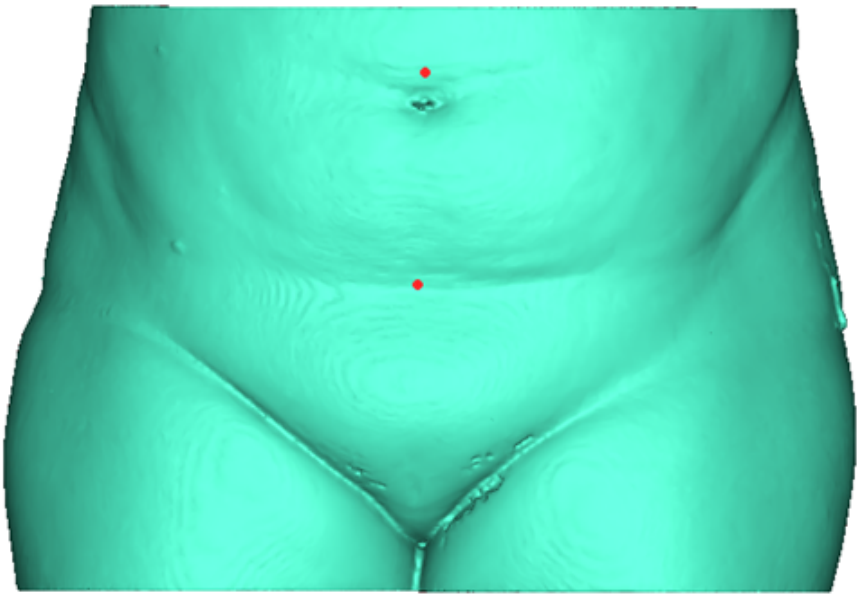

63. Left (and Right) lateral point: 6 centimeter dorsolateral from the anterior superios iliac spine (ASIS) and 3 centimeter cranial from that point.

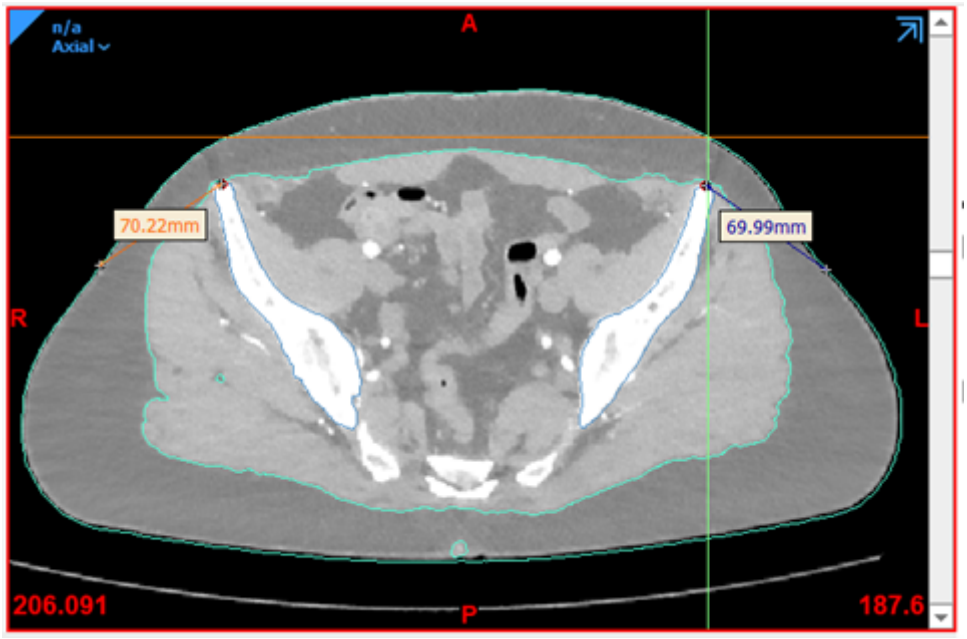

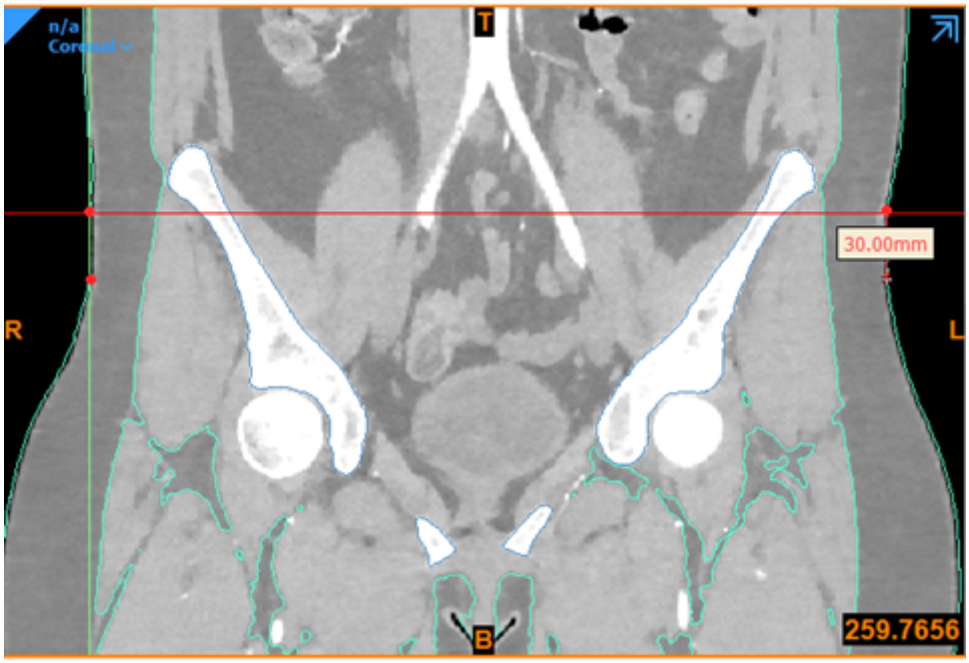

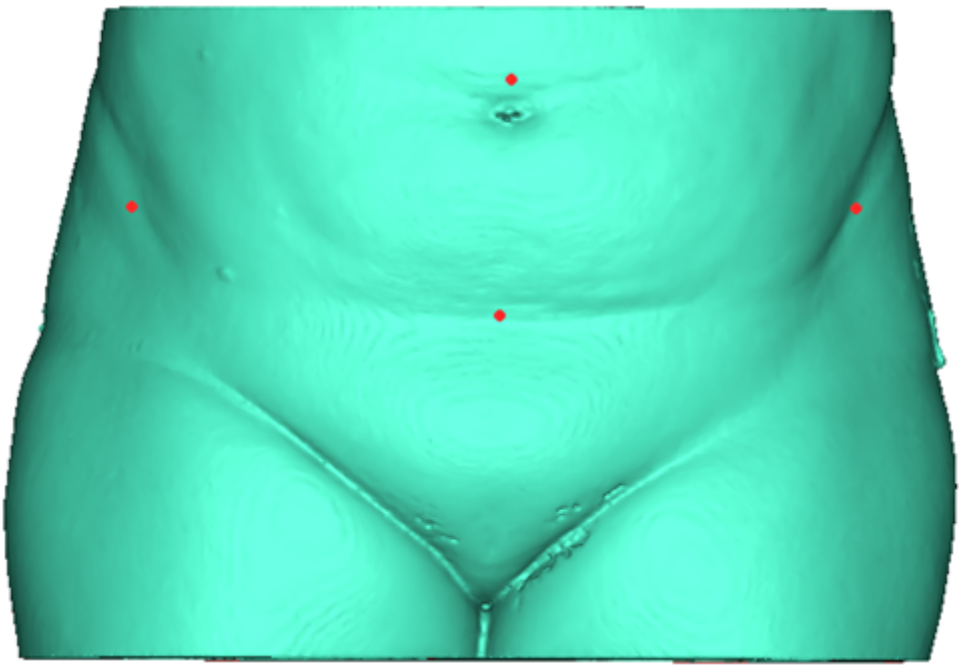

64. Next, go to “ANALYZE” and select “Freeform Surface”. Create an inferior and superior border for the DIEP flap using this freeform surface. Ensure that the superior border cuts cranial towards the rectus muscle as performed during surgery.

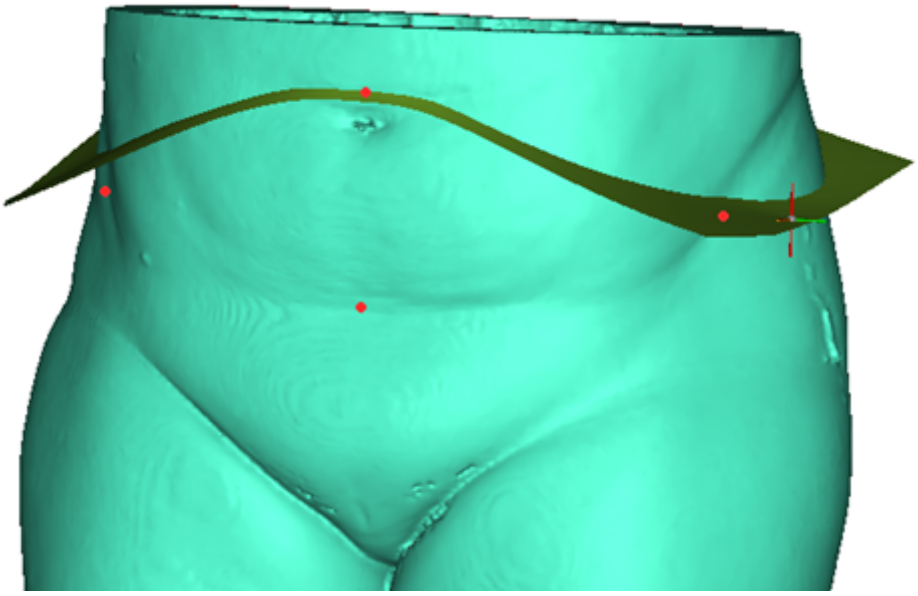

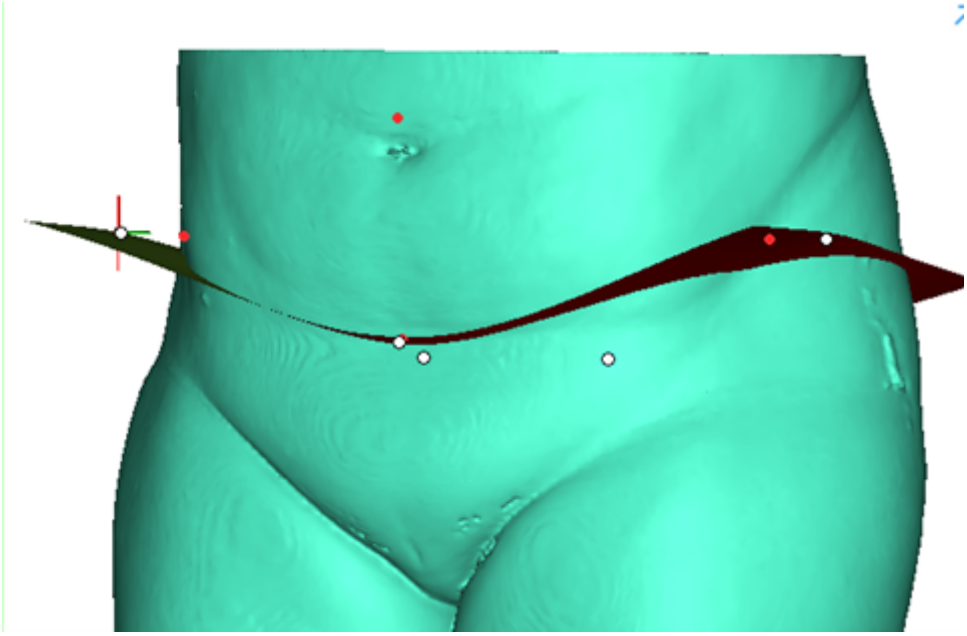

65. Next, go to “3D TOOLS” and select “Cut”. Select the part “Cutis” stored in folder DIEP flap and select the superior border as cutting object.
66. Select the part which includes the DIEP flap and repeat the previous step with the “inferior border”.
67. Name this finalized and cut part from the DIEP flap “DIEP flap” and create a duplicate. Store this duplicate in the folder “Final parts”.
68. If necessary, adjust the final part by transforming the part to a mask and adjust the mask using the “Edit Mask” tool under “SEGMENT”

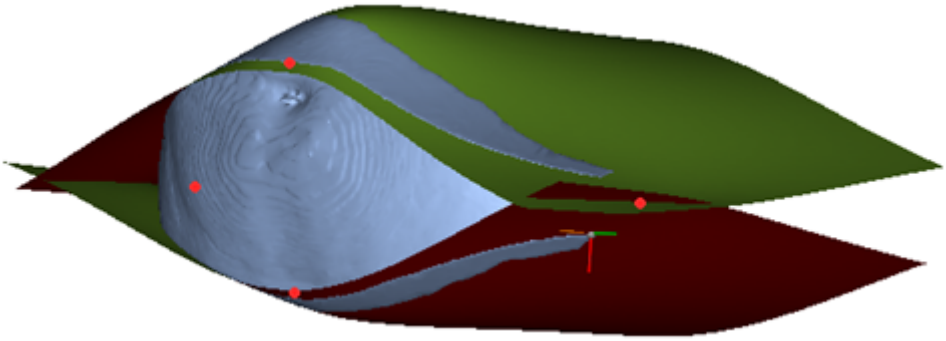

Export

69. Go to “FILE” and then to “Export”. Export all parts saved in the folder “Final parts” to 3-matic: Pelvis, Skin, Rectus Abdominis Muscle, Cutis, left DIEP, right DIEP, (left SIEA, right SIEA) and DIEP flap.

3-matic and Mimics Viewer

70. Adjust the colors of all parts to the desired color and opacity.
71. Safe this file as “DIEP_case_xx-date”
72. Go to: Mimics Viewer (materialise.net)
73. Upload the 3-matic file.

You have now reached the end of the segmentation protocol.

C

Raw Data

Table C.1: raw data of questionnaire and DIEP flap weigth outcomes

Castor EDC ID	110008	110009	110010	110011	110012
Participant characteristics					
Function description	Staff-Member	Resident (AIOS)	Staff-Member	Resident	Staff-Member
Experience of resident	N/A	10 to 20	N/A	>30	N/A
System Usability Scale (SUS) CTA					
SUS item					
1	5	4	2	4	5
2	1	2	2	2	2
3	5	3	4	3	4
4	1	2	1	4	1
5	3	4	3	2	4
6	3	2	2	4	2
7	2	4	4	2	3
8	2	1	2	1	3
9	4	4	4	4	4
10	4	4	2	5	4
SUS score CTA	70	70	70	47.5	70
Perforator Characteristics CTA					
item					
1 Location in the flap	4	3	4	4	5
2 Calibre	4	3	2	2	3
3 Intramuscular course	4	4	3	3	5
System Usability Scale (SUS) XR					
SUS item					
1	5	4	4	5	3
2	3	2	4	3	2
3	3	4	2	2	3
4	2	2	4	1	1
5	5	4	5	4	4
6	4	2	1	1	2
7	5	4	4	5	4
8	3	2	2	1	3
9	4	4	2	4	3
10	3	2	3	2	2
SUS score XR	67.5	75	57.5	80	67.5
Perforator Characteristics XR					
item					
1 Location in the flap	5	4	5	5	4
2 Calibre	5	4	3	4	3
3 Intramuscular course	3	4	4	4	4
Additional Value XR in addition to CTA					
item					
1	5	4	3	5	2
2	5	4	4	4	4
Predicted flap volume 2D method (cm)					
a, sagittal view - the base (b)	19.4	21.9	20.5	18.0	19.0
b, axial view - the height (h)	17.3	13.8	16.3	16.7	14.5
c, axial view - the thickness (t)	3.8	2.4	1.3	4.0	3.8
Predicted flap weight 2D method (g)	1275	725	434	1202	1047